mRNA-mediated induced regeneration of the corneal endothelium

Authors:

Maxwell Marshall[1], Lisa Ohman[1], Bakary Samasa[3], Tyler Papp[1], Parhiz Hamideh[1] & Panteleimon Rompolas[1,2,3,5]†

Affiliations:

[1] Department of Dermatology, University of Pennsylvania Perelman School of Medicine, Philadelphia, PA, USA

[2] Department of Ophthalmology, Scheie Eye Institute, University of Pennsylvania Perelman School of Medicine, Philadelphia, PA, USA

[3] Department of Cell and Developmental Biology, University of Pennsylvania Perelman School of Medicine, Philadelphia, PA, USA

[4] Department of Medicine, University of Pennsylvania Perelman School of Medicine, Philadelphia, PA, USA.

[5] Institute for Regenerative Medicine, University of Pennsylvania, Philadelphia, PA, USA

† To whom correspondence should be addressed:

Email: rompolas@pennmedicine.upenn.edu

Tel: 215-573-4002

Abstract

Loss of vision due to corneal endothelial dysfunction affects millions worldwide and has limited treatment options. Here we present a proof of concept for a therapeutic approach that aims to enhance regeneration of the corneal endothelium by inducing proliferation of quiescent cells in vivo, using modified mRNA technology. To test the efficacy of this strategy we developed a mouse model to analyze corneal endothelial regeneration by longitudinal live imaging, using two-photon microscopy. The mouse corneal endothelium displayed complete cellular quiescence and a decline in cell density with aging, consistent with human data. Limited proliferation of corneal endothelial cells was observed during injury repair but was insufficient to restore the tissue to pre-injury levels. Treatment via intracameral injection of five modified mRNAs, encoding for proteins involved in cell cycle activation, induced transient proliferation in corneal endothelial cells in the absence of injury and led to an increase in tissue cell density. This approach may offer a paradigm for enhancing the regenerative response in organs with limited endogenous ability.

Main Text

The corneal endothelium is a tissue with limited documented regenerative activity [**1**]. Corneal endothelial cells regulate the optical transparency of the cornea by maintaining the stroma in a state of relative dehydration, through their ion pumping activity and barrier function [**2, 3**]. Corneal endothelial cells are developmentally derived from the neural crest and establish a tissue monolayer in the posterior corneal surface, which becomes mitotically inactive postnatally and into adulthood, through well studied mechanisms of contact inhibition and insulation from growth signals [**4-6**]. A progressive decline in the number of corneal endothelial cells due to aging or other factors can lead to corneal edema and loss of vision, due to a decompensated ion pumping capacity [**7**]. Corneal endothelial disorders are a leading cause of reduced vision and blindness, affecting ~4% of the population over 40 [**8**]. The current standard of care for treating corneal endothelial dysfunction is penetrating or posterior lamellar keratoplasty, which presents a challenge due to the complexity and cost of the procedure, and worldwide shortages in donor tissue [**9**, **10**]. A promising strategy to prevent the disease and restore vision, is to modulate intrinsic molecular pathways to promote corneal endothelial cell proliferation, in order to rejuvenate the tissue [**11**]. Modified mRNA technology can be used to transiently alter the protein expression program of cells in vivo, offering an appealing vehicle for the implementation of this therapeutic strategy [**12**]. Despite the exciting prospects, the pace of research to develop new therapies for corneal endothelial dysfunction is hampered by inherent inefficiencies of current experimental models. Toward addressing this unmet clinical need, we recently demonstrated a methodology for intravital imaging of the intact mouse eye, by two-photon microscopy, which enables the direct longitudinal visualization of the corneal tissue at a single-cell resolution [**13**]. This system allows to interrogate the activity of corneal endothelial cells in vivo and measure direct outcomes of experimental interventions in real time. Therefore, we leveraged the power of our live imaging approach to develop an mRNA-based therapeutic, to promote corneal endothelial regeneration, and test its efficacy in a pre-clinical mouse model.

Proliferation of corneal endothelial cells, from humans as well as other species, has been demonstrated to occur under certain conditions, such as ex vivo or in cell culture [**14-16**].

However, the activity of corneal endothelial cells in vivo is still poorly understood. To date, rabbits and other large animals have been the preferred models for research of the corneal endothelium due to their large eyes and close approximation of the human phenotype, of limited corneal endothelial regeneration [**17**]. Despite the perceived weaknesses, the mouse is readily amenable to genetic manipulation; we therefore, sought to capitalize on contemporary genetic tools to investigate different facets of corneal endothelial physiology, by live imaging. The small size of the mouse eye is also advantageous for our system, which can rapidly image the whole cornea and capture cellular behaviors across the entire organ. Thus, we directly imaged the eyes of live mice, using genetically encoded fluorescent reporters to resolve the fine morphology of the corneal endothelium at a single cell resolution (**Fig 1A, S1A-C**). The morphological characteristics of mouse corneal endothelial cells recapitulate that of the human tissue, including a hexagonal apical surface and ruffled basal cell membranes (**Fig S2**). Common clinical presentations of corneal endothelial dystrophies include: 1) a gradual cell loss, and corresponding changes in the shape and size of individual cells with age, and 2) the appearance of "guttae"; extracellular excrescences that interrupt the lateral contacts between endothelial cells [**18, 19**]. Live imaging of mouse corneas during different stages of adulthood, showed a consistent cell loss, accompanied by cellular polymegathism and pleomorphism that correlated with age (**Fig 1B-F; S1**). Using a membrane reporter to directly visualize the cell-cell contacts within the endothelial layer, we also observed "guttae" like structures, that appeared only in aged mice (**Fig 1E, S2**). Another unique feature of aged corneas revealed by this analysis, was a pronounced change in nuclear morphology (**Fig 1G-I**), which may imply changes in chromatin organization and gene expression, as previously proposed for other cell types [**20**]. These data validated the relevance and sensitivity of our approach and demonstrated that the physiology of corneal endothelial cells can be accurately analyzed by live imaging.

The observed decline in cell density of the mouse corneal endothelium as a function of aging suggests lack of proliferative activity under normal physiology, at least at sufficient levels to replenish the tissue. Clinical evidence of partial regeneration after stripping of the corneal endothelium, are consistent with earlier studies in animal models, which suggest that corneal endothelial cells have mitotic potential that can be activated by injury [**21-24**]. While a

mechanism for injury repair of the corneal endothelium is generally accepted, the cellular activities involved in this process and the distinct contribution of individual cells to the regeneration of the tissue have not been fully resolved. Elucidating the conditions that can activate the cell cycle in vivo, is critical for informing effective therapeutic strategies aiming at induced proliferation in the corneal endothelium. To address this, we developed an in vivo injury model to induce localized damage to corneal endothelium and analyze the cellular behaviors during the repair process by longitudinal live imaging. We found that non-penetrating, superficial scraping of the epithelium causes rupture of the endothelium in the posterior corneal surface, likely due to acute stromal edema from the loss of epithelial barrier (**Fig 2A, S3, S4**). By re-imaging the same corneas over time, we captured the dynamics of the injury repair across the entire corneal tissue. As predicted, the corneal epithelium fully regenerated, and was morphologically indistinguishable from the pre-injury state (**Fig S4**). The corneal endothelium was also able to repair the injury, re-establishing a seemingly intact monolayer of cells (**Fig 2A, S3, S4**). However, detailed analysis revealed that the cell density was significantly reduced compared to pre-injury levels (**Fig 2B, C, S3**). Moreover, individual corneal endothelial cells were enlarged at various degrees (**Fig 2B**).

The observed phenotype was more pronounced in the center of the tissue, near the site of injury, suggesting a repair mechanism driven primarily by cell migration and enlargement at the wound edge. Alternatively - or in concert - cell proliferation may be limited to the periphery of the corneal endothelium, where a population with stem cell properties is proposed to reside [**25-26**]. To directly answer this question, we used mice that express a cell-cycle reporter (CyclinB1-GFP) to capture proliferating cells during the tissue repair, by live imaging. We validated the specificity and faithful kinetics of the reporter by imaging the mitotically active corneal epithelium (**Fig S5A**). Pre-injury, GFP was not detected in the corneal stroma or the endothelium. Proliferating cells appeared in the corneal endothelium 24 hours post-injury; their numbers peaked at 2 days and proliferation became again undetectable in the tissue three days after injury (**Fig 2D, S5B**). This is consistent with the timing of the repair process and the reestablishment of the corneal endothelial monolayer. Aged mice harboring the cell cycle reporter, showed a similar number of GFP+ cells in the corneal endothelium after injury,

compared to young mice. These data directly demonstrate the in vivo proliferative potential of corneal endothelial cells that is maintained with age. More importantly, they show that under these conditions, proliferation is consistently induced in cells near the wound margins, suggesting that the local environment is critical for cell cycle activation and argues against a spatially restricted stem cell population.

Next, we sought to improve upon the sensitivity of our in vivo assays to detect cellular outcomes in response to external inputs with high spatiotemporal resolution. The gold standard in Regenerative Medicine research is the use of Cre/LoxP-based in vivo lineage tracing systems with cell-type specific genetic drivers [**27**]. To date, such approaches have not been widely implemented to studying the regeneration of the corneal endothelium, primarily due to lack of validated endothelial-specific Cre drivers. To address this, we leveraged our expertise with in vivo lineage tracing models and devised a strategy to induce loxP genomic recombination using Cre-encoding modified mRNA (**Fig 3A**). When delivered systemically, using lipid nanoparticle vehicles, Modified mRNAs are endocytosed primarily by hepatocytes, but localized induced expression has been demonstrated when mRNAs are injected in situ [**28**]. We hypothesized that local delivery of modified mRNA would be especially advantageous for the corneal endothelium, due to the protected environment of the anterior eye chamber and the relative slow turnover of the aqueous humor that would aid the retention and endocytosis of the mRNA cargo by corneal endothelial cells. To test this, we performed intracameral injection of GFP-encoding mRNA in wild type mice and validated expression by live imaging (**Fig 3A, S6**). We observed robust GFP signal in approximately 5-20% of corneal endothelial cells, that peaked 24 hours after injection and persisted at detectable levels for up to 7 days after injection (**Fig 3B, S6**). Elsewhere in the anterior eye segment, expression was detected only in the iris but was completely absent from the corneal epithelium and stroma, or the lens (**Fig S6**). Expression was also not observed in the non-injected contralateral eye (**Fig S6**).

To track the activity of individual corneal endothelial cells under normal tissue physiology and to resolve their contribution to tissue repair, we performed in vivo lineage tracing by longitudinal live imaging. For this, we used mice harboring a fluorescent Cre reporter and induced

recombination and clonal labeling by local injection of modified Cre-encoding mRNA (**Fig 3C**). Imaging of the corneas at 24 hours after injection confirmed Cre-induced recombination and labeling of corneal endothelial cells (**Fig 3D**). Furthermore, no new recombination events were observed after 24 hours, indicating that mRNA uptake is limited within this time window. Re-imaging the same corneas at different timepoints after labeling we confirmed the near absolute quiescence of corneal endothelial cells, as the labeled cells remained virtually unchanged in their original positions within the tissue several months after labeling (**Fig 3D**). Next, we wanted to track corneal endothelial cells during injury, to resolve the cellular activities involved in the repair process. By imaging the corneas at daily intervals after the injury we captured profound changes in corneal endothelial cells at the wound margins (**Fig S7**). These cells rapidly migrated towards the wound bed, becoming enlarged and extending filopodia-like structures (**Fig S7**). Through their concerted activity, the edges of the wound were brought together and adhered within three days after injury, effectively closing the wound. After this point, and once the continuity of the monolayer was re-established, no further changes were observed in the number, location, or morphology of individual cells within the corneal endothelium (**Fig S7**). In our previous experiments, we demonstrated the existence of proliferating cells during injury repair with an in vivo cell cycle reporter; however, due to the dynamic nature of this reporter we could only capture a snapshot of cells that are in the G2/M phase of the cell cycle at the time of imaging. To analyze the full extent of proliferation and resolve the history and spatiotemporal dynamics of mitotically active corneal endothelial cells, we developed a multi-color lineage tracing strategy which would allow us to track individual cells and their progeny with high accuracy (**Fig S8A)**. After injection of the Cre-encoding mRNA, the corneas were imaged to document the location of labeled cells, and then re-imaged after one month, which confirmed that the tissue was at steady state with no evidence of proliferation or other changes to the corneal endothelial cells (**Fig S8B)**. By tracking individual cells after induction of injury we obtained definitive evidence that corneal endothelial cells are activated and can undergo one or more cycles of cell division before returning into a quiescent state (**Fig 3E, S8B)**. Importantly, we found that activation of corneal endothelial cells occurs exclusively at the wound margins, while the rest of the tissue is maintained in a quiescent state throughout the repair process and thereafter (**Fig 3E, S8B)**. We confirmed this by implementing an orthogonal approach, using

photo-labeling as an unbiased way to track cells proximal and distal to the wound margin (**Fig S9)**.

To this point, we developed and validated a powerful live imaging-based in vivo model to investigate corneal endothelial regeneration. Using this system, we demonstrated that in the absence of a growth stimulus, the tissue exists in a quiescent non-replenishing state, and thus declining with age. We also show evidence that corneal endothelial cells can be induced to activate their cell cycle, and that this is a universal property of the tissue and not restricted to a particular subpopulation of progenitor cells. Our data demonstrating the efficacy of mRNA-mediated expression of exogenous proteins in corneal endothelial cells in vivo, empowered us to develop a therapeutic strategy to re-activate the cell cycle activity in the absence of injury. Our hypothesis was that induced expression of key enzymes and transcription factors would activate the relevant signaling pathways to allow the corneal endothelial cells to undergo mitosis. To test this hypothesis, we performed a literature search and selected 5 pro-growth factors: Cdk4 and ccnd1(cyclin D1) form a complex that promotes progression of the cell cycle [**29,30**]. Sox2 and Myc, two of the Yamanaka factors for somatic cell re-programming, are known to promote proliferation in various cell types, including in corneal endothelial cells [**31,33**]. Yap is a downstream effector of the Hippo pathway, that is critical for mediating contact inhibition growth [**34,35**].

Our strategy to test the efficacy of these factors to induce proliferation of corneal endothelial cells, and document any potential adverse effects, involved concurrent lineage tracing of the cells that incorporated the mRNAs (**Fig 4A)**. To validate this strategy, we first tested injecting a combination of mRNAs that encode traceable reporters (GFP + mCherry and GFP + Cre-recombinase) and confirmed that cells which expressed one reporter aways expressed the other, suggesting that a mix of mRNA molecules is equally delivered and expressed by the corneal endothelial cells in vivo (**Fig S10)**. Thus, we used a Cre-encoding mRNA combined with a Cre reporter mouse line, as a surrogate to visualize and track the corneal endothelial cells that express the 5 growth factors, encoded by the injected mRNA cocktail. 24 hours after injection cells that received the mRNA cocktail underwent mitosis (**Fig 4B-D, S11)**. The control corneas that only

received the Cre and GFP-encoding mRNAs remained virtually unchanged with no evidence of proliferation, consistent with our previous lineage tracing experiments (**Fig 4B-D, S11)**. Corneal endothelial cells that responded to the treatment with the mRNA growth factors maintained a normal morphology and expression of typical corneal endothelial markers **(Fig 4E)**. We reproduced these results using a different mouse model, which also confirmed that activation of the cell cycle (CyclinB1-GFP) was specific to cells that expressed the growth-factors after mRNA injection (**Fig 4F, S12)**. It is important to note that in corneas which received the mRNA cocktail, proliferation was induced throughout the endothelium and in areas distal from the site of injection, suggesting that this was independent from potential injury cues. Moreover, no further proliferation was observed in subsequent re-imaging of the same corneas (**Fig 4B-F, S11, S12)**.

These experimental data provide a proof of concept that corneal endothelial cells can be induced to proliferate in vivo, by modulating key molecular pathways, using modified mRNA delivered directly into the anterior eye chamber (**Fig 4G**). Despite the potential oncogenic nature of the factors tested here, the safety profile of modified mRNA-based therapies for corneal endothelial dysfunction is advantageous, due to the lack of genomic integration and inherent instability and short-half of mRNAs in the cytoplasm. This is in line with our data showing a transient uptick in cell proliferation during the first 24 hours after injection, and a quick return to quiescence. The stability and performance of therapeutic mRNAs can be improved, by 5' and 3' sequence optimizations, synthetic capping, and incorporation of modified nucleosides [**36-38**]. High efficiency and improved specificity for the in vivo delivery of the mRNA cargo can also be achieved with the use of optimally formulated lipid nanoparticles and incorporation of cell-specific antibodies to minimize potential off-target effects, as recently demonstrated [**39**]. Furthermore, due to the relative low risk of the treatment, dosing of the delivered mRNAs can be incremental and adjusted to achieve optimal increase in cell numbers that restore the corneal endothelium to its optimal density. While many of these modifications were incorporated into this study, future work is needed to systematically test these parameters to achieve optimal clinical outcomes. We envision that the in vivo models and mRNA-based methodologies developed for the purposes of this study will serve as a paradigm for basic research and enable

new therapeutic platforms to address unmet clinical needs for corneal endothelial and other ocular diseases. Proliferation-inducing strategies using modified mRNA technology may also have far-reaching applications for other organs affected by cellular attrition due to aging or disease.

Acknowledgments

We thank George Cotsarelis, Ken Zaret, Jonathan Epstein and Jean Bennet for their feedback and critical review of this manuscript. This study was partially supported by a seed grant from Penn Health Tech and the Regenerative Ophthalmology Program, made possible by a generous donation from Richard and Carolyn Sloane. We also acknowledge the support of the Institute for Regenerative Medicine and the entire stem cell community at Penn. P.R. was supported by grants from NIH/NEI (R01EY030599) and from the American Cancer Society (RSG1803101DCC).

Author contributions: P.R. conceptualized the study, designed and performed the experiments. M.M. performed the breeding and genotyping of mice. L.O. and B.S. performed histological analyses. T.P and H.P. assisted with the mRNAs IVT and Western blot analysis. All authors discussed results and participated in the manuscript preparation and editing. P.R. supervised the study and wrote the manuscript.

Competing interests: A provisional patent application has been filed for “Compositions and methods for regenerating corneal endothelium”.

Data and materials availability: Data sets and reagents presented in this study are available from the corresponding author upon request.

Figure Legends

Figure 1. Intravital imaging of the mouse corneal endothelium. A) Experimental approach to directly visualize the corneal endothelium in live mice by two-photon microscopy. Schematic shows an exploded view of the three cellular compartments of the cornea and example of an en face view of the live mouse corneal endothelium**.** B) Images of the mouse corneal endothelium from a 3-month and 22-month old mouse, using a nuclear in vivo reporter (*Rosa26-nT*omato). C) Quantification of cell density in the corneal endothelium as a function of age [N = 40, 8 corneas per age group, P < 0.0001; one-way ANOVA]. D) Quantification of cell density in the same corneas imaged at the indicated ages [N = 4 corneas, P < 0.0024; two-way ANOVA]. E) Images of the mouse corneal endothelium from a 6-month and 24-month-old mouse, using a membrane in vivo reporter (*Rosa26-mT*omato). Yellow arrows indicate guttae-like structures between corneal endothelial cells. Image on the right shows a high magnification view an aged corneal endothelium with a characteristic guttae structure. F) Quantification of cellular pleomorphism in in the corneal endothelium as a function of age [N = 254 cells from 6 corneas per age group, P < 0.0001; one-way ANOVA]. G) 3-dimensional rendering of corneal endothelial nuclei from young and aged corneas.H) Quantification of nuclear perimeter of corneal endothelial cells as a function of age [N = 241 nuclei from 8 corneas, P < 0.0001; one-way ANOVA]. I) Quantification of nuclear circularity [(4π (Area)/(Perimeter^2)] of corneal endothelial cells as a function of age [N = 241 nuclei from 8 corneas, P < 0.0001; one-way ANOVA]. Scale bar 50μm.

Figure 2. Incomplete regeneration of the corneal endothelium after injury. A) Representative time points from injury repair of the corneal endothelium captured by longitudinal live imaging. Top panels show low magnification views of the entire eye, before, during and after injury; brightfield (left) and wide field epifluorescent (right)**.** Bottom panels show a maximum projection en face view of the corneal endothelium. B) Representative high magnification views of the central and peripheral corneal endothelium, from the same eye imaged before and after injury. C) Quantification of cell density in the central and peripheral corneal epithelium before and after injury. Each bar pair represents a different cornea analyzed before and after injury [N = 3-8 fields/cornea, P < 0.0015/0.0001/0.0052/0.78/0.34/0.73, paired t-

test]. D) Representative high magnification views of the corneal endothelium taken before and two days after injury. A globally-expressed red fluorescent reporter with nuclear localization (*Rosa26-nTnG*) is used to visualize all corneal endothelial cells in the tissue. Actively proliferating cells are visualized by green fluorescence by expression of the in vivo cell cycle reporter (*CyclinB1-GFP*). Scale bars 200μm (A), 50μm (B, D).

Figure 3. Cellular dynamics of corneal endothelial injury repair. A) Experimental design for induced protein expression in corneal endothelial cells in vivo, via intracameral injection modified mRNA. B) Example of GFP expression in corneal endothelial cells 24 hours after modified mRNA injection. C) Experimental design of in vivo lineage tracing of corneal endothelial cells via in situ delivery of Cre-recombinase encoding modified mRNA and longitudinal live imaging. D) Representative low and high magnification images of the same mouse eye imaged 24 hours after mRNA injection (Labeling) and re-imaging at the indicated time points. Top panels show side views of the whole mouse eye (left-peripheral cornea, right-central cornea). E) Examples of multi-color in vivo lineage tracing of corneal endothelial cells, using the *Rosa26-confetti* reporter. Left panels show low and high magnification views of the wound margins, taken at one and ten days after injury. Arrows show representative single corneal endothelial cells at the wound margin that divided during this timeframe. Right panels show equivalent areas of the same corneas located distally from the wound margin. Scale bars 50μm.

Figure 4. mRNA-mediated cell cycle activation in the corneal endothelium. A) Experimental design for induced proliferation of corneal endothelial cells in vivo, via intracameral injection of pro-growth protein-encoding mRNAs. Cells that incorporate the mRNAs are traced by longitudinal live imaging to analyze outcomes. B) Quantification of change in the number of labeled cells that receive either the Cre-recombinase alone (Control), or plus the mRNA cocktail of pro-growth proteins (Cocktail). [N = 7 corneas, $P < 0.0001$; two-way ANOVA] C) Representative examples from a lineage tracing experiment following mRNA injection of Cre-recombinase alone (Control), or plus the mRNA cocktail of pro-growth proteins. The same corneas were re-imaged at the indicated timepoints. Cells that incorporate the mRNAs switch

from a nuclear Tomato to a nuclear GFP signal (*Rosa26-nTnG*) and their fate can be traced longitudinally. Cells that receive only the Cre mRNA remain quiescent while those that also receive the cocktail of the five mRNAs undergo cell divisions. D) Quantification of change in total endothelial cell density of corneas injected with either the Cre-recombinase alone (Control), or plus the mRNA cocktail of pro-growth proteins (Cocktail). The same corneas were re-imaged at the indicated timepoints. Each bar pair represents a different cornea imaged before and after treatment [N = 5 measurements per cornea per timepoint; Cocktail: P = 0.0013(1), 0.0147(2), 0.0002(3); Control: P = 0.5 (1), 0.01(2), 0.33(3); paired t-test]. E) Whole mount immunolabeling with the endothelial marker ZO-1, of corneas from *Rosa26-nTnG* mice collected ten days after injection with mRNA encoding for Cre plus the cocktail of pro-growth proteins. Asterisks show cells that have incorporated and expressed the mRNA as indicated but the switch from a nuclear Tomato to a nuclear GFP signal (*Rosa26-nTnG* allele). F) Example of a lineage tracing experiment using the in vivo cell cycle reporter (CyclingB1-GFP) in conjunction with the Cre-reporter (*Rosa26-tdTomato*). Cells that receive the mRNA cocktail are the only ones that show positive GFP signal, indicating selective activation of the cell cycle in these cells. G) Schematic of the mRNA-mediated proliferation of corneal endothelial cells. Endothelial cells that incorporate the mRNAs after the intracameral injection are show in red. After treatment endothelial cells that express the proteins encoded by the mRNA cocktail undergo a limited round of proliferation which leads to a stable increase of cell density in the endothelial layer.

Supplementary Figure 1. A) Schematic of the mammalian eye and a magnified view of the structural organization of the cornea. B) Experimental approach for deconstructing the cornea in vivo by optical sectioning with two-photon microscopy. C) Representative low (left) and high (right) magnification images of the epithelium, stroma and endothelium, from a young and old mouse, taken at the indicated depths from the surface of the cornea. A globally expressed, membrane-localized fluorescent reporter (*Rosa26-mTomato*) was used to resolve the fine tissue morphology in vivo. Scale bars 200μm, 50μm.

Supplementary Figure 2. High magnification images of the corneal endothelium from a young and aged mouse. Images were acquired using 2μm thick serial optical sections. Corresponding

models illustrate the distinct cell-cell contacts and membrane organization of the basal and apical surfaces of the corneal endothelium (left panels; adapted from *He et al. Sci Rep 2016*). A globally expressed, membrane-localized fluorescent reporter (*Rosa26-mTomato*) was used to resolve the fine tissue morphology in vivo. Scale bar 50μm.

Supplementary Figure 3. Representative low and high magnification maximal projections of the endothelial layers (bottom panels) and corresponding side views of the entire thickness of the cornea (top panels), taken at the indicated time points before and after injury. A globally expressed, nuclear-localized red fluorescent reporter (*Rosa26-nTomato*) was used to resolve cell numbers and density in vivo. The stromal extracellular matrix is visualized by Second Harmonic Generation (SHG) and shown in cyan. Scale bars 200μm.

Supplementary Figure 4. Representative low magnification maximal projections of the entire mouse eye (top panel; side view), epithelial and endothelial layers (middle panels, en face view) and corresponding high magnification views of the central and peripheral corneal endothelium (bottom panels, en face view), taken at the indicated time points before and after injury. A globally expressed, membrane-localized red fluorescent reporter (*Rosa26-mTomato*) was used to resolve tissue and cell morphology in vivo. The stromal extracellular matrix is visualized by Second Harmonic Generation (SHG) and shown in green (top panel). Scale bars 200μm.

Supplementary Figure 5. A) Validation of the cell cycle reporter used to capture corneal endothelial proliferation in vivo. Top left panel shows the sequence elements of the transgenic reporter. Expression of GFP recapitulates the kinetics of the endogenous cyclin B1 enzyme, with a peak signal intensity during the G2/M phases of the cell cycle. Bottom left panel shows representative frames from a time sequence, which depict actively cycling cells in the live corneal epithelium. Red arrows show cells that complete mitosis, in whose daughter cells the GFP signal quickly becomes undetectable. Right panel shows a low magnification en face view of the basal layer of the corneal epithelium, where the number and distribution of basal progenitors that are actively proliferating can be visualized by green fluorescence. A globally

expressed, nuclear-localized red fluorescent reporter (*Rosa26-nTomato*) was used as a counterstain to resolve cell numbers and density in vivo. B) Representative low magnification en face view of the corneal endothelium (bottom panels) and corresponding side views of the entire thickness of the cornea (top panels), taken at the indicated time points before and after injury. Proliferating corneal endothelial cells can be visualized by green fluorescence (*CyclinB1-GFP*). The stromal extracellular matrix is visualized by Second Harmonic Generation (SHG) and depicted in cyan (XZ views). Scale bar 200μm.

Supplementary Figure 6. A) Validation of efficacy and specificity of protein expression in the corneal endothelium by modified mRNA, delivered in vivo by intracameral injection. A GFP encoding modified mRNA was injected into one eye of a live mouse and the eye was imaged 24 hours after injection. Expression of GFP was detected in the corneal endothelium but not the lens of the injected eye or anywhere in the un-injected contralateral eye. Two-photon imaging using 750nm laser wavelength was used to generate metabolite autofluorescence and was used as a counterstain to visualize unlabeled cells in magenta. B) Representative low magnification en face views of the same corneas taken at the indicated timepoints. Expression of GFP persists up to seven days after injection of the modified mRNA. C) Co-expression of GFP and mCherry in corneal endothelial cells after injection of a cocktail consisting of equal amounts of mRNA encoding for each fluorescent protein. Scale bar 50μm.

Supplementary Figure 7. Representative low (top panels) and high (bottom panels) magnification views of the wounded corneal endothelium taken at the indicated time points during injury repair. Cre-recombinase encoding mRNA was injected before the injury to mark corneal endothelial cells and track their activity during repair. A globally expressed, membrane-localized cre reporter (*Rosa26-mTmG*) was used to resolve tissue and cell morphology in vivo and to mark cells which express the Cre-recombinase with mGFP. Scale bars 200μm.

Supplementary Figure 8. A) Validation of multi-color labeling of corneal endothelial cells. Diagram shows the sequence elements of the *Rosa26-confetti* reporter and the possible

recombination events that result in ten unique color combinations when mice homozygous for the two confetti alleles are used. Imaging of the corneal endothelium after injection of cre-encoding modified mRNA confirmed these theoretical color labels expressed stochastically in single corneal endothelial cells. B) Representative low (top panels) and high (bottom panels) magnification views of the corneal endothelium taken at the indicated time points before and after injury. Cre-recombinase encoding mRNA was injected before the injury to mark corneal endothelial cells and track their activity during repair. Red and yellow squares indicate cells located proximal and distal to the wound margin, respectively. Note that labeled cells remain quiescent for at least two months before injury, but only those proximal to the wound margin become activated and proliferate after injury. Scale bars 200μm.

Supplementary Figure 9. A) Experimental strategy for un-biased lineage tracing of corneal endothelial cells by in vivo photo-labeling and longitudinal live imaging. B) Representative low (top panels) and high (bottom panels) magnification views of the corneal endothelium taken at the indicated time points after injury. Equivalent groups of cells were photo-labeled at various distances from the center of the cornea (1-3) as well as proximal to the wound margin (4). Imaging at 850nm was used to visualize the pre-activated state of the globally expressed PAGFP reporter and was used as a counterstain to visualize unlabeled cells in the tissue. Imaging at 930nm illuminates only cells in which the PAGFP was irreversibly photo-activated. The same corneas were re-imaged to track changes in the labeled cells after injury. Note that labeled cells distal to wound edge remain quiescent and don't directly contribute to injury repair. Scale bars 500μm.

Supplementary Figure 10. A) Sequence elements of mRNAs used in this study. See Material and Methods for more information. B) Western blot analysis of protein expression in 392T cells transfected with the indicated mRNAs.

Supplementary Figure 11. Lineage tracing time course to analyze induced proliferation of corneal endothelial cells in vivo, following intracameral injection of pro-growth protein-

encoding mRNAs. Cells that incorporate the mRNAs are traced by longitudinal live imaging to analyze outcomes. Panels show representative low and high magnification en face views of the corneal endothelium at the indicated timepoints from mRNA injection of Cre-recombinase alone (Control), or plus the mRNA cocktail of pro-growth proteins. Cells that incorporate the mRNAs switch from a nuclear Tomato to a nuclear GFP signal (*Rosa26-nTnG*) and their fate can be traced longitudinally. Red squares indicate the same cells imaged during the time course and depicted in high magnification in the bottom panels. Scale bars 200μm.

Supplementary Figure 12. Lineage tracing time course to analyze induced proliferation of corneal endothelial cells in vivo, following intracameral injection of pro-growth protein-encoding mRNAs. Panels show representative low and high magnification en face views of the corneal endothelium at the indicated timepoints from mRNA injection of the mRNA cocktail of pro-growth proteins. The mice used in these experiments express an in vivo cell cycle reporter (*CyclingB1-GFP*) in conjunction with the Cre-reporter (*Rosa26-tdTomato*). Cells that incorporate the mRNAs are labeled with red fluorescence and their fate can be traced longitudinally. The same corneas where imaged 24 hours after mRNA injection and again ten days later. After the final imaging the corneas where dissected, stained with DAPI to visualize the nuclei of corneal endothelial cells and imaged again as whole mounts. White squares indicate the same cells imaged during the time course and depicted in high magnification in panels 1-3. Scale bars 200μm.

Methods

Mice

All procedures involving animal subjects were performed with the approval of the Institutional Animal Care and Use Committee (IACUC) of the University of Pennsylvania and were consistent with the guidelines set forth by the ARVO Statement for the Use of Animals in Ophthalmic and Vision Research. $R26^{loxp\text{-}stop\text{-}loxp\text{-}tdTom}$, $R26^{loxp\text{-}tdTom\text{-}stop\text{-}loxp\text{-}EGFP}$, $R26^{loxp\text{-}nTom\text{-}stop\text{-}loxp\text{-}nGFP}$, $R26^{lox\text{-}stop\text{-}loxp\text{-}Confetti}$ and $Pgk1CyclinB1^{\text{-}GFP}$ mice were obtained from The Jackson Laboratory. $R26^{PAGFP}$ reporter mice were generated by crossing the $E2a^{Cre}$ with $R26^{loxp\text{-}stop\text{-}loxp\text{-}PAGFP}$ lines, obtained from The Jackson Laboratory, to achieve germline transmission of the recombined allele and ubiquitous expression of the PAGFP reporter. All mice that were used in this study were bred for multiple generations into a Crl:CD1(ICR) mixed background. Mice were housed in a temperature and light-controlled environment and received food and water *ad libitum*. Up to 5 mice of the same sex and similar age were housed in a cage. Mice were provided Bed-o'Cobs (The Andersons Lab Bedding), a porous cob material, as bedding and Shred-n'Rich nestlets (The Andersons Lab Bedding) for nesting and enrichment.

Intravital imaging of the mouse eye

Preparation of the mice for intravital imaging of the eye was performed with the following amendments to the previously described protocol (Rompolas et al. 2016). Mice were initially anesthetized with IP injection of ketamine/xylazine cocktail (0.1 ml / 20 g body weight; 87.5 mg / kg Ketamine, 12.5 mg / kg Xylazine). A deep plane of anesthesia was verified by checking pedal reflexes. The mouse head was stabilized with a custom-made stereotaxic apparatus that includes palate bar and nose clamp but no ear bars. Precision, 3-axis micro-manipulators are used to adjust the head tilt so that the eye to be imaged is facing up. A drop of eye gel (0.3 % Hypromellose) was used as an optically neutral interface between the eye and a glass coverslip, and to prevent dryness and irritation to the tissue during the anesthesia and imaging procedure. After preparation and mounting is complete, the stage is placed on the microscope platform under the objective lens. A heating pad is used to keep a stable body temperature and vaporized isoflurane is delivered through a nose cone to maintain anesthesia for the duration of the imaging process. After each imaging

session, the eyes were rinsed with PBS and the mice were monitored and allowed to recover in a warm chamber before returned to the housing facility.

Imaging equipment and acquisition settings

Image acquisition was performed with an upright Olympus FV1200MPE microscope, equipped with a Chameleon Vision II Ti:Sapphire laser. The laser beam was focused through 10X, 20X or 25X objective lenses (Olympus UPLSAPO10X2, N.A. 0.40; UPLSAPO20X, N.A. 0.75; XLPLN25XWMP2, N.A. 1.05) and. Emitted fluorescence was collected by two multi-alkali and two gallium arsenide phosphide (GaAsP) non-descanned detectors (NDD). The following wavelengths were collected by each detector: NDD1 419-458 nm; NDD1 458–495 nm; GaAsP-NDD1 495–540 nm; GaAsP-NDD2 575–630 nm. GFP and Tomato reporters were excited at 930 nm and their signal was collected by GaAsP-NDD1 and GaAsP-NDD2, respectively. Second harmonic generation (SHG) signal was generated using 850 nm or 930 nm excitation wavelengths and detected by NDD1 or NDD2, respectively. Serial optical sections were acquired in 2–5 μm steps, starting from the surface of the eye and capturing the entire thickness of the cornea (epithelium ~40 μm, stroma/endothelium ~80 μm). Expanded views of the cornea and limbus were obtained by acquiring a grid of sequential optical fields-of-view that were automatically stitched into one high-resolution tiled image using the microscope manufacturer software. Multi-day tracing experiments were done by re-imaging the same field-of-view or the entire eye at the indicated times after the initial acquisition. For each time point, inherent landmarks within the cornea, including the organization of the vasculature and collagen fibers (SHG), were used to consistently identify the limbus and navigate back to the original regions. Macroscopic images of the mouse eye were acquired under brightfield and fluorescence with an Olympus MVX10 Fluorescent Macro Zoom microscope fitted with Hamamatsu Orca CCD camera for digital imaging.

Photo-labeling

Photo-labeling experiments with the *R26*^{PAGFP} reporter mice were carried out with the same equipment and imaging setup as used for acquisition. The pre-activated form of the fluorescent proteins was visualized by exciting with 850 nm wavelength and emission signal was collected in GaAsP-NDD1 (495-540nm). Excitation with 930 nm verified that no signal is emitted by the

reporters before activation. Photo-labeling was achieved by scanning a defined region-of-interest (ROI) at the plane of the basal layer of the epithelium, with the laser tuned to 750nm wavelength, for 5-10 sec, using 5-10% laser power. The z-plane was then moved down to the corneal endothelium, which served as a reference, and the same ROI was used for photo-labeling cells in that layer. Immediately after photo-activation, a series of optical sections, with a range that includes the entire thickness of the cornea, were acquired using the same acquisition settings as for GFP. Visualizing the signal of the activated form of PAGFP only within the ROI confirmed the successful photo-labeling of basal epithelial or endothelial cells. Following the initial image acquisition immediately after photo-labeling the same eyes were re-imaged at the indicated times to evaluate the changes of the labeled epithelial population and their movements compared to the endothelial reference cell group.

Wounding assay

Corneal epithelial debridement wounds were generated as previously described (Chan & Werb 2015). Mice were initially anesthetized with IP injection of ketamine/xylazine cocktail and their eyes imaged under brightfield and fluorescence microscopy. Mice where then placed on a heating pad and observed under an Olympus SZ61 dissecting microscope. After topical application of Proparacaine the epithelium from the central part of the cornea was removed with an Algerbrush II ophthalmic brush to generate a scrape wound of 1.5 mm in diameter. The eyes were imaged again before the mice were allowed to recover.

Intracameral injections

Adult mice ranging from 3-22 months of age mice were used for this procedure. For analgesia 1-2 drops of topical .5% proparacaine eye drops were instilled to each eye before the procedure. Mice were initially anesthetized with IP injection of ketamine/xylazine cocktail and kept warm using a temperature-controlled heating pad throughout the whole procedure. A deep plane of anesthesia was verified by checking pedal reflexes. The mouse head was stabilized by means of a palate bar and nose clamp and using a special sterotaxic apparatus that does not require the use of ear bars. Using precision micro-manipulators, the head angle was adjusted so that the treated eye was facing upwards. The pupils were dilated with .5% tropicamide ophthalmic drops and the treated eye was examined under a stereomicroscope to ensure that the pupil is fully dilated and

that the ocular muscles are relaxed so that there is no eye movement. The absence of eye movements ensures stability during the injection. A diluted betadine solution was applied topically using a 1ml syringe to the ocular surface and fornices. For the injection a custom-made microinjection apparatus was used that attaches directly to the same heated mounting platform that is used for intravital imaging. The microinjector is composed of a hydraulic pump (Eppendorf CellTram Oil) connected to a 1mm inner diameter PTFE flexible tubing. A fitting adaptor connects the tubing to a single-use, sterile 31-gauge insulin pen needle (CareTouch). When attached to the tubing the microneedle is connected to a 3-axis manual micromanipulator to precisely control its movement during the injection. Using the microinjector pump a 5µl solution is loaded into the syringe, ensuring that no air bubbles enter the system or are present at the tip of the needle. Using the micromanipulators, the needle is guided to the mouse eye at a 45° angle, anteriorly relative to the limbus. The cornea is gently punctured so that the tip of the microneedle enters the anterior chamber, ensuring that the loaded microneedle remains at a 45° angle relative to the limbus during the puncture. Contact with the iris or the lens should be avoided. During this process the eye may need to be supported with a pair of disposable plastic tweezers from the opposite side. Using the microsyringe pump, ~ 1.5 µl of solution is injected into the anterior chamber. This amount is injected gradually over 30 seconds before withdrawing the microneedle. Antibiotic ointment (Bacitracin Zinc and Polymyxin B Sulfate Ophthalmic Ointment USP) was applied to the treated eyes as prophylactic.

Modified mRNA design, synthesis and encapsulation

The constructs for the in vitro transcription (IVT) of cdk4, ccnd1, myc, sox2 and yap- encoding mRNAs were custom designed and synthesized by VectorBuilder using a template plasmid carrying a T7 promoter. A 5’ aptamer sequence for eIF4G binding was inserted between the T7 promoter and the start codon to optimize ribosome binding and translation initiation [**38**]. Downstream from the ORF and stop codon a 3’UTR sequence was inserted that consists of a combined 3’UTR from mitochondrial encoded 12S rRNA (mtRNR1) and the amino-terminal enhancer of split mRNA (AES), which has been reported to significantly improve mRNA stability and expression [**30**]. A minimum of 30 nucleotide long poly-A tail was also encoded into the DNA template. Template pDNA was linearized and ARCA-capped IVT-mRNA was

produced using the T7 HiScribe kit from NEB, pseudo-uridine was incorporated into the reaction, and the product was Poly(a) tailed enzymatically using the manufacture's recommendations. IVT-mRNA was then cellulose-purified to remove dsRNA products from the reaction. For validation of the IVT-mRNAs, 293T cells were cultured in 10% HI-FBS/1% PennStrep, then transfected with either luciferase IVT-mRNA or test IVT-mRNA. Cells were collected in cold DPBS, and pelleted. Cell pellets were lysed with 1x RIPA + protease inhibitor cocktail. 40μg protein per sample was denatured in LDS reducing buffer containing BME at 70 degrees Celsius for 10 minutes. Protein was loaded into 4-12% Bis-Tris SDS Bolt gel and dry-transferred using iBlot instrument to nitrocellulose membrane. Blots were blocked in 5% milk/TBST overnight before incubating with primary and secondary anti-rabbit-HRP antibodies. Blots were developed using Immobilon ECL Ultra Western HRP Substrate and captured on Amersham Imager 600. Blots were stripped, blocked overnight, and re-probed with anti-GAPDH antibody. For control experiments, 5-methoxyuridine, nucleoside-modified CleanCap mRNAs encoding for EGFP, mCherry and Cre-recombinase were used (Trilink Biotechnologies). Encapsulation of modified mRNAs for intracameral injection was performed using Lipofectamine Messenger Max transfection reagent (Thermo Fischer) for following the manufacturer recommendations. A final concentration of 20 ng/μl of encapsulated mRNA in Opti-MEM medium (Thermo Fischer) was used for the in vivo injections.

Quantitative image analysis

Raw digital files from 2-photon imaging were acquired and saved in the OIB format using the microscope manufacturer's software (FLUOVIEW, Olympus USA). To capture extended fields-of-view that encompass the entire ocular surface epithelium, including the cornea, limbus and conjunctiva, a tiling method was used to reconstruct a single image from multiple full-thickness serial optical sections using the microscope acquisition software. Typically, to image the entire eye using the 10X objective lens, the microscope defines a square area consisting of 2 x 2 (XY) field-of-view with 10% overlap between them. Using the motorized platform, the microscope automatically acquires the four fields-of-view in a sequential pattern and uses information from the overlapping margins to stitch the individual field-of-view into a single image. Raw image files were imported into ImageJ/Fiji (NIH) using Bio-Formats or to Imaris (Bitplane) for further

analysis. For cell counts and quantitative clonal analyses, supervised image segmentation and blob detection was performed on individual optical sections. Identified blobs were manually validated and their number, size and signal intensity as mean grey values were measured.

Statistical analysis

Sample sizes were not pre-determined, but are similar with what was reported previously (Farrelly et al. 2021). Data were collected and quantified randomly, and their distribution was assumed normal, but this was not formally tested. Lineage tracing, photo-labeling and wounding experiments were successfully reproduced under similar conditions using different mouse cohorts. Unless stated otherwise in the legends, data presented in the figures are from a single cohort of at least three mice, imaged in tandem, using identical experimental parameters. The values of "N" (sample size) refer to data points obtained from all mice within the cohort, unless otherwise indicated, and are provided in the figure legends. Statistical calculations and graphical representation of the data were performed using the Prism software package (GraphPad). Data are expressed as percentages or mean ± S.E.M and unpaired Student's *t*-test was used to analyze data sets with two groups, unless otherwise stated in the figure legends. For all analyses, P-values < 0.05 were designated as significant and symbolized in figure plots as $*P < 0.05$, $**P < 0.01$, $***P < 0.001$, $****P < 0.0001$, with precise values supplied in figure legends. No data were excluded from the analysis.

References

1. Joyce NC. Proliferative capacity of corneal endothelial cells. Exp Eye Res. 2012 Feb;95(1):16-23. doi: 10.1016/j.exer.2011.08.014. Epub 2011 Aug 30. PMID: 21906590; PMCID: PMC3261346.
2. Tuft SJ, Coster DJ. The corneal endothelium. Eye (Lond). 1990;4 (Pt 3):389-424. doi: 10.1038/eye.1990.53. PMID: 2209904.
3. Maurice DM. The location of the fluid pump in the cornea. J Physiol. 1972 Feb;221(1):43-54. doi: 10.1113/jphysiol.1972.sp009737. PMID: 5016991; PMCID: PMC1331318.
4. Murphy C, Alvarado J, Juster R, Maglio M. Prenatal and postnatal cellularity of the human corneal endothelium. A quantitative histologic study. Invest Ophthalmol Vis Sci. 1984 Mar;25(3):312-22. PMID: 6698749.
5. Bourne WM, Nelson LR, Hodge DO. Central corneal endothelial cell changes over a ten-year period. Invest Ophthalmol Vis Sci. 1997 Mar;38(3):779-82. PMID: 9071233.
6. Yee RW, Matsuda M, Schultz RO, Edelhauser HF. Changes in the normal corneal endothelial cellular pattern as a function of age. Curr Eye Res. 1985 Jun;4(6):671-8. doi: 10.3109/02713688509017661. PMID: 4028790.
7. Eghrari AO, Riazuddin SA, Gottsch JD. Fuchs Corneal Dystrophy. Prog Mol Biol Transl Sci. 2015;134:79-97. doi: 10.1016/bs.pmbts.2015.04.005. Epub 2015 Jul 15. PMID: 26310151.
8. Whitcher JP, Srinivasan M, Upadhyay MP. Corneal blindness: a global perspective. Bull World Health Organ. 2001;79(3):214-21. Epub 2003 Jul 7. PMID: 11285665; PMCID: PMC2566379.
9. Gain P, Jullienne R, He Z, Aldossary M, Acquart S, Cognasse F, Thuret G. Global Survey of Corneal Transplantation and Eye Banking. JAMA Ophthalmol. 2016 Feb;134(2):167-73. doi: 10.1001/jamaophthalmol.2015.4776. PMID: 26633035.
10. Klintworth GK. Corneal dystrophies. Orphanet J Rare Dis. 2009 Feb 23;4:7. doi: 10.1186/1750-1172-4-7. PMID: 19236704; PMCID: PMC2695576.
11. Arras W, Vercammen H, Ní Dhubhghaill S, Koppen C, Van den Bogerd B. Proliferation Increasing Genetic Engineering in Human Corneal Endothelial Cells: A Literature Review. Front Med (Lausanne). 2021 Jun 29;8:688223. doi: 10.3389/fmed.2021.688223. PMID: 34268324; PMCID: PMC8275833.
12. Weissman D. mRNA transcript therapy. Expert Rev Vaccines. 2015 Feb;14(2):265-81. doi: 10.1586/14760584.2015.973859. Epub 2014 Oct 31. PMID: 25359562.
13. Farrelly O, Suzuki-Horiuchi Y, Brewster M, Kuri P, Huang S, Rice G, Bae H, Xu J, Dentchev T, Lee V, Rompolas P. Two-photon live imaging of single corneal stem cells reveals compartmentalized organization of the limbal niche. Cell Stem Cell. 2021 Jul 1;28(7):1233-1247.e4. doi: 10.1016/j.stem.2021.02.022. Epub 2021 May 12. PMID: 33984283; PMCID: PMC8559309.

14. Zhu C, Joyce NC. Proliferative response of corneal endothelial cells from young and older donors. Invest Ophthalmol Vis Sci. 2004 Jun;45(6):1743-51. doi: 10.1167/iovs.03-0814. PMID: 15161835.
15. Silverstein AM, Khodadoust AA, Prendergast RA. Desquamation of corneal endothelial cells. Invest Ophthalmol Vis Sci. 1982 Mar;22(3):351-8. PMID: 7061208.
16. Rolev K, Coussons P, King L, Rajan M. Experimental models of corneal endothelial cell therapy and translational challenges to clinical practice. Exp Eye Res. 2019 Nov;188:107794. doi: 10.1016/j.exer.2019.107794. Epub 2019 Sep 10. PMID: 31518569.
17. Park S, Leonard BC, Raghunathan VK, Kim S, Li JY, Mannis MJ, Murphy CJ, Thomasy SM. Animal models of corneal endothelial dysfunction to facilitate development of novel therapies. Ann Transl Med. 2021 Aug;9(15):1271. doi: 10.21037/atm-20-4389. PMID: 34532408; PMCID: PMC8421955.
18. Borboli S, Colby K. Mechanisms of disease: Fuchs' endothelial dystrophy. Ophthalmol Clin North Am. 2002 Mar;15(1):17-25. doi: 10.1016/s0896-1549(01)00016-5. PMID: 12064077.
19. Cibis GW, Weingeist TA, Krachmer JH. Traumatic corneal endothelial rings. Arch Ophthalmol. 1978 Mar;96(3):485-8. doi: 10.1001/archopht.1978.03910050261014. PMID: 415710.
20. Lans H, Hoeijmakers JH. Cell biology: ageing nucleus gets out of shape. Nature. 2006 Mar 2;440(7080):32-4. doi: 10.1038/440032a. PMID: 16511477.
21. Iovieno A, Neri A, Soldani AM, Adani C, Fontana L. Descemetorhexis Without Graft Placement for the Treatment of Fuchs Endothelial Dystrophy: Preliminary Results and Review of the Literature. Cornea. 2017 Jun;36(6):637-641. doi: 10.1097/ICO.0000000000001202. PMID: 28410355.
22. Van Horn DL, Sendele DD, Seideman S, Buco PJ. Regenerative capacity of the corneal endothelium in rabbit and cat. Invest Ophthalmol Vis Sci. 1977 Jul;16(7):597-613. PMID: 873721.
23. Matsubara M, Tanishima T. Wound-healing of corneal endothelium in monkey: an autoradiographic study. Jpn J Ophthalmol. 1983;27(3):444-50. PMID: 6656008.
24. Befanis PJ, Peiffer RL Jr, Brown D. Endothelial repair of the canine cornea. Am J Vet Res. 1981 Apr;42(4):590-5. PMID: 7332117
25. Espana EM, Sun M, Birk DE. Existence of Corneal Endothelial Slow-Cycling Cells. Invest Ophthalmol Vis Sci. 2015 Jun;56(6):3827-37. doi: 10.1167/iovs.14-16030. PMID: 26066751; PMCID: PMC4468414.
26. Correll MH, Crouzet E, Gain P, He Z, Udsen MS, Kiilgaard JF, de la Cour MD, Heegaard S, Thuret G. In Vivo Labeling and Tracking of Proliferating Corneal Endothelial Cells by 5-Ethynyl-2'-Deoxyuridine in Rabbits. Transl Vis Sci Technol. 2021 Sep 1;10(11):7. doi: 10.1167/tvst.10.11.7. PMID: 34478491; PMCID: PMC8419885.
27. Kretzschmar K, Watt FM. Lineage tracing. Cell. 2012 Jan 20;148(1-2):33-45. doi: 10.1016/j.cell.2012.01.002. PMID: 22265400.
28. Zangi L, Lui KO, von Gise A, Ma Q, Ebina W, Ptaszek LM, Später D, Xu H, Tabebordbar M, Gorbatov R, Sena B, Nahrendorf M, Briscoe DM, Li RA, Wagers AJ, Rossi DJ, Pu WT, Chien KR. Modified mRNA directs the fate of heart progenitor cells

and induces vascular regeneration after myocardial infarction. Nat Biotechnol. 2013 Oct;31(10):898-907. doi: 10.1038/nbt.2682. Epub 2013 Sep 8. PMID: 24013197; PMCID: PMC4058317.

29. Tchakarska G, Sola B. The double dealing of cyclin D1. Cell Cycle. 2020 Jan;19(2):163-178. doi: 10.1080/15384101.2019.1706903. Epub 2019 Dec 29. PMID: 31885322; PMCID: PMC6961668.
30. Tchakarska G, Sola B. The double dealing of cyclin D1. Cell Cycle. 2020 Jan;19(2):163-178. doi: 10.1080/15384101.2019.1706903. Epub 2019 Dec 29. PMID: 31885322; PMCID: PMC6961668.
31. Takahashi K, Yamanaka S. Induction of pluripotent stem cells from mouse embryonic and adult fibroblast cultures by defined factors. Cell. 2006 Aug 25;126(4):663-76. doi: 10.1016/j.cell.2006.07.024. Epub 2006 Aug 10. PMID: 16904174.
32. Kwan KY, Shen J, Corey DP. C-MYC transcriptionally amplifies SOX2 target genes to regulate self-renewal in multipotent otic progenitor cells. Stem Cell Reports. 2015 Jan 13;4(1):47-60. doi: 10.1016/j.stemcr.2014.11.001. Epub 2014 Dec 11. PMID: 25497456; PMCID: PMC4297878.
33. Chang YK, Hwang JS, Chung TY, Shin YJ. SOX2 Activation Using CRISPR/dCas9 Promotes Wound Healing in Corneal Endothelial Cells. Stem Cells. 2018 Dec;36(12):1851-1862. doi: 10.1002/stem.2915. Epub 2018 Oct 15. Erratum in: Stem Cells. 2019 Jun;37(6):E4. PMID: 30270540.
34. Joyce NC, Harris DL, Mello DM. Mechanisms of mitotic inhibition in corneal endothelium: contact inhibition and TGF-beta2. Invest Ophthalmol Vis Sci. 2002 Jul;43(7):2152-9. PMID: 12091410.
35. Gumbiner BM, Kim NG. The Hippo-YAP signaling pathway and contact inhibition of growth. J Cell Sci. 2014 Feb 15;127(Pt 4):709-17. doi: 10.1242/jcs.140103. PMID: 24532814; PMCID: PMC3924201.
36. Karikó K, Buckstein M, Ni H, Weissman D. Suppression of RNA recognition by Toll-like receptors: the impact of nucleoside modification and the evolutionary origin of RNA. Immunity. 2005 Aug;23(2):165-75. doi: 10.1016/j.immuni.2005.06.008. PMID: 16111635.
37. Karikó K, Muramatsu H, Welsh FA, Ludwig J, Kato H, Akira S, Weissman D. Incorporation of pseudouridine into mRNA yields superior nonimmunogenic vector with increased translational capacity and biological stability. Mol Ther. 2008 Nov;16(11):1833-40. doi: 10.1038/mt.2008.200. Epub 2008 Sep 16. PMID: 18797453; PMCID: PMC2775451.
38. Tusup M, French LE, De Matos M, Gatfield D, Kundig T, Pascolo S. Design of in vitro Transcribed mRNA Vectors for Research and Therapy. Chimia (Aarau). 2019 May 29;73(6):391-394. doi: 10.2533/chimia.2019.391. PMID: 31118121.
39. Rurik JG, Tombácz I, Yadegari A, Méndez Fernández PO, Shewale SV, Li L, Kimura T, Soliman OY, Papp TE, Tam YK, Mui BL, Albelda SM, Puré E, June CH, Aghajanian H, Weissman D, Parhiz H, Epstein JA. CAR T cells produced in vivo to treat cardiac injury. Science. 2022 Jan 7;375(6576):91-96. doi: 10.1126/science.abm0594. Epub 2022 Jan 6. PMID: 34990237.

40. Orlandini von Niessen AG, Poleganov MA, Rechner C, Plaschke A, Kranz LM, Fesser S, Diken M, Löwer M, Vallazza B, Beissert T, Bukur V, Kuhn AN, Türeci Ö, Sahin U. Improving mRNA-Based Therapeutic Gene Delivery by Expression-Augmenting 3' UTRs Identified by Cellular Library Screening. Mol Ther. 2019 Apr 10;27(4):824-836. doi: 10.1016/j.ymthe.2018.12.011. Epub 2018 Dec 18. PMID: 30638957; PMCID: PMC6453560.

Figure 1

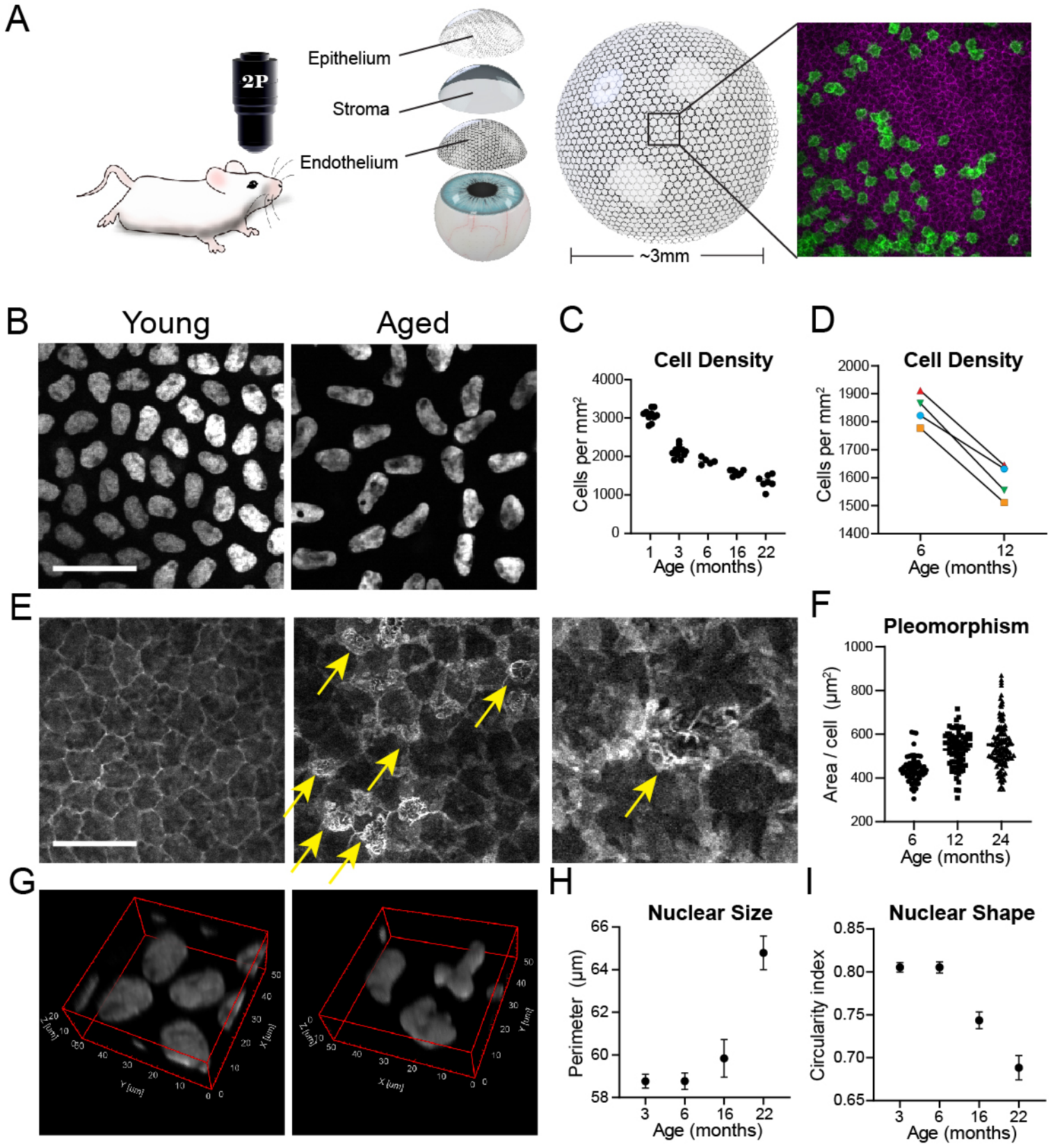
A
2P
Epithelium
Stroma
Endothelium
~3mm
B
Young
Aged
C
Cell Density
Cells per mm²
Age (months)
D
Cell Density
Cells per mm²
Age (months)
E
F
Pleomorphism
Area / cell (µm²)
Age (months)
G
H
Nuclear Size
Perimeter (µm)
Age (months)
I
Nuclear Shape
Circularity index
Age (months)

Figure 2

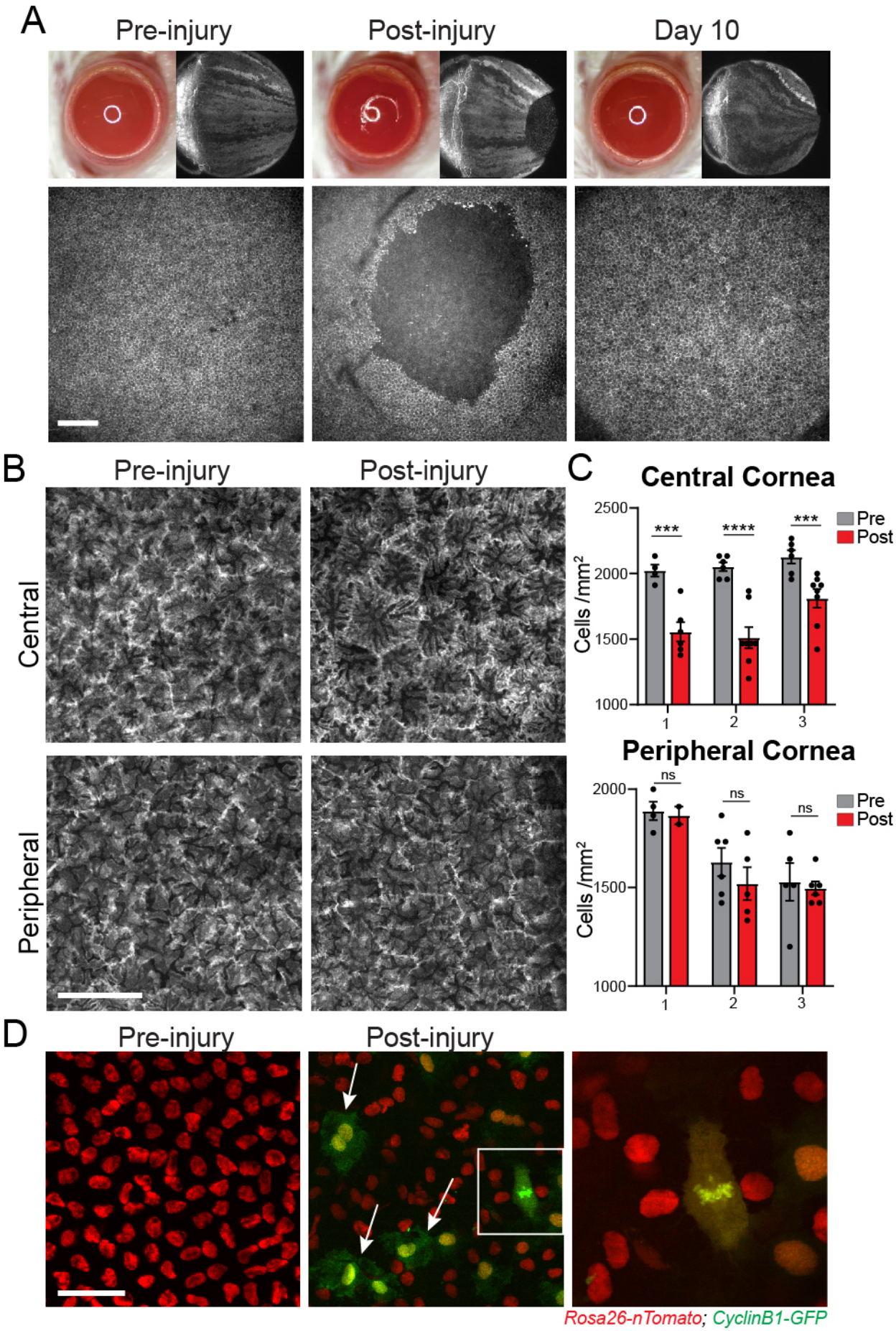
A
Pre-injury
Post-injury
Day 10
B
Pre-injury
Post-injury
Central
Peripheral
C
Central Cornea
Cells /mm²
2500
2000
1500
1000
***
****
***
1
2
3
Pre
Post
Peripheral Cornea
ns
ns
ns
D
Pre-injury
Post-injury
Rosa26-nTomato; CyclinB1-GFP

Figure 3

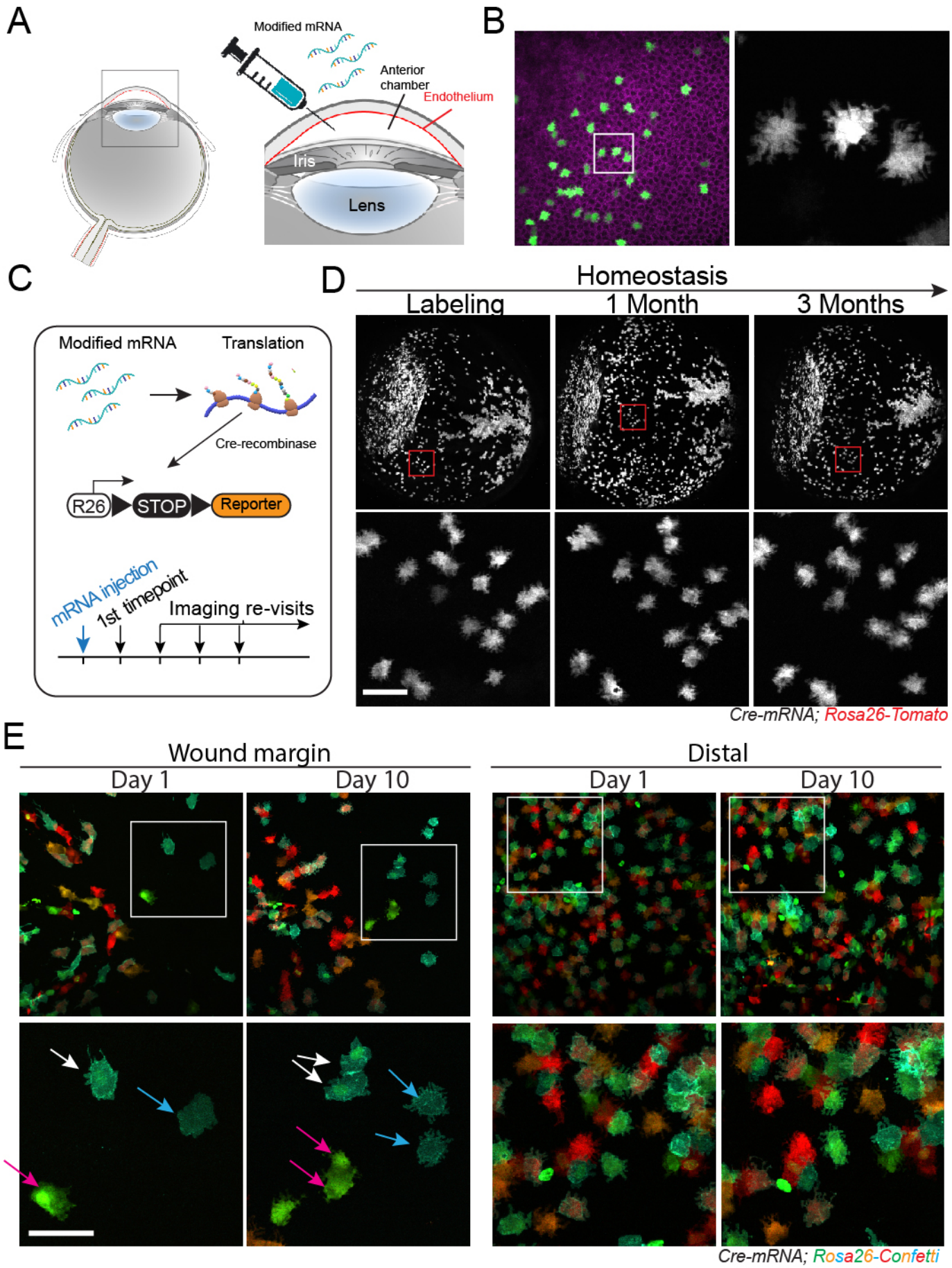
A
Modified mRNA
Anterior chamber
Endothelium
Iris
Lens
B
C
Modified mRNA
Translation
Cre-recombinase
R26
STOP
Reporter
mRNA injection
1st timepoint
Imaging re-visits
D
Homeostasis
Labeling
1 Month
3 Months
Cre-mRNA; Rosa26-Tomato
E
Wound margin
Day 1
Day 10
Distal
Day 1
Day 10
Cre-mRNA; Rosa26-Confetti

Figure 4

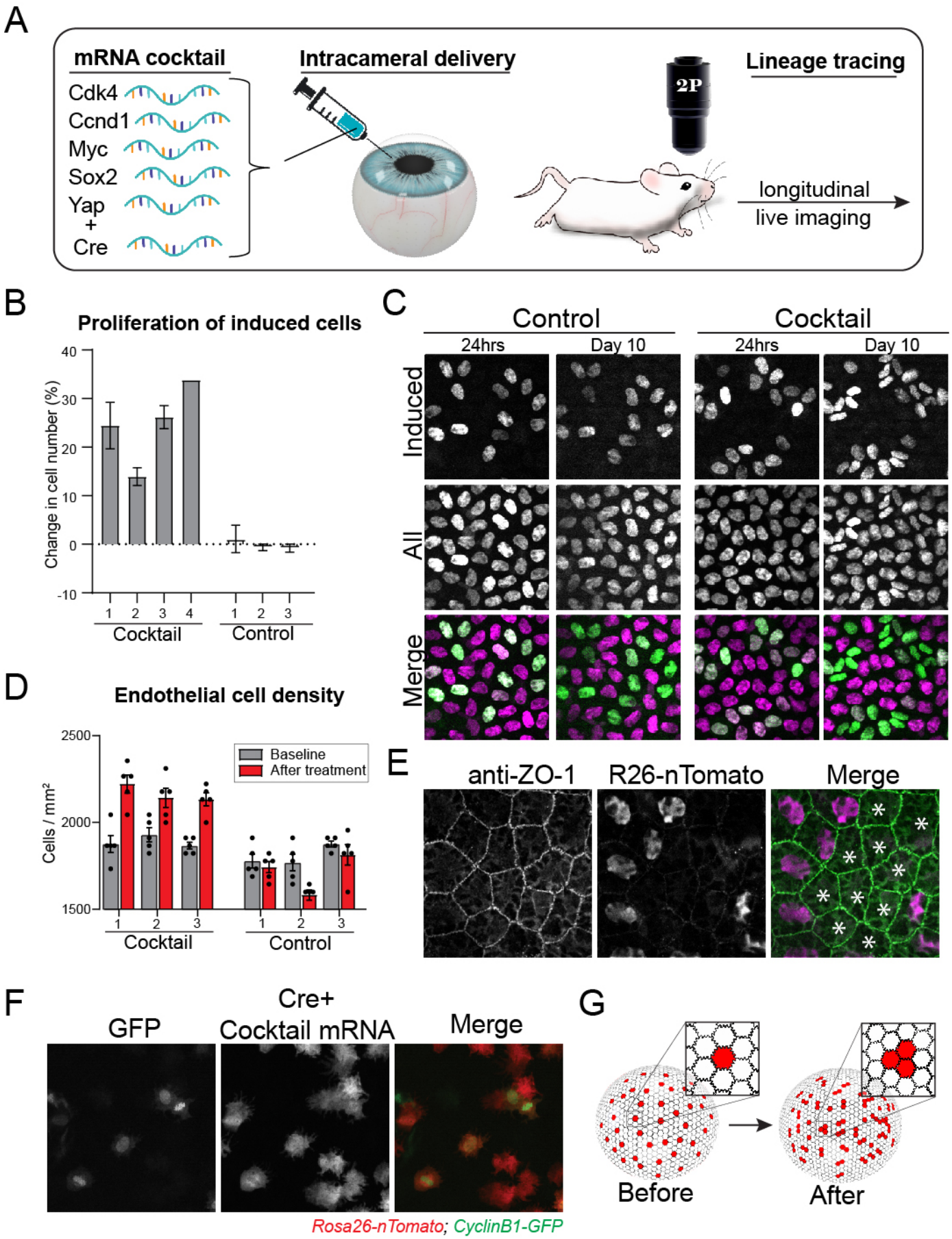
A
mRNA cocktail
Cdk4
Ccnd1
Myc
Sox2
Yap
+
Cre
Intracameral delivery
2P
Lineage tracing
longitudinal
live imaging
B
Proliferation of induced cells
Change in cell number (%)
40
30
20
10
0
-10
1 2 3 4
Cocktail
1 2 3
Control
C
Control
Cocktail
24hrs
Day 10
24hrs
Day 10
Induced
All
Merge
D
Endothelial cell density
Cells / mm²
2500
2000
1500
Baseline
After treatment
1 2 3
Cocktail
1 2 3
Control
E
anti-ZO-1
R26-nTomato
Merge
F
GFP
Cre+
Cocktail mRNA
Merge
Rosa26-nTomato; CyclinB1-GFP
G
Before
After

Supplementrary figure 1

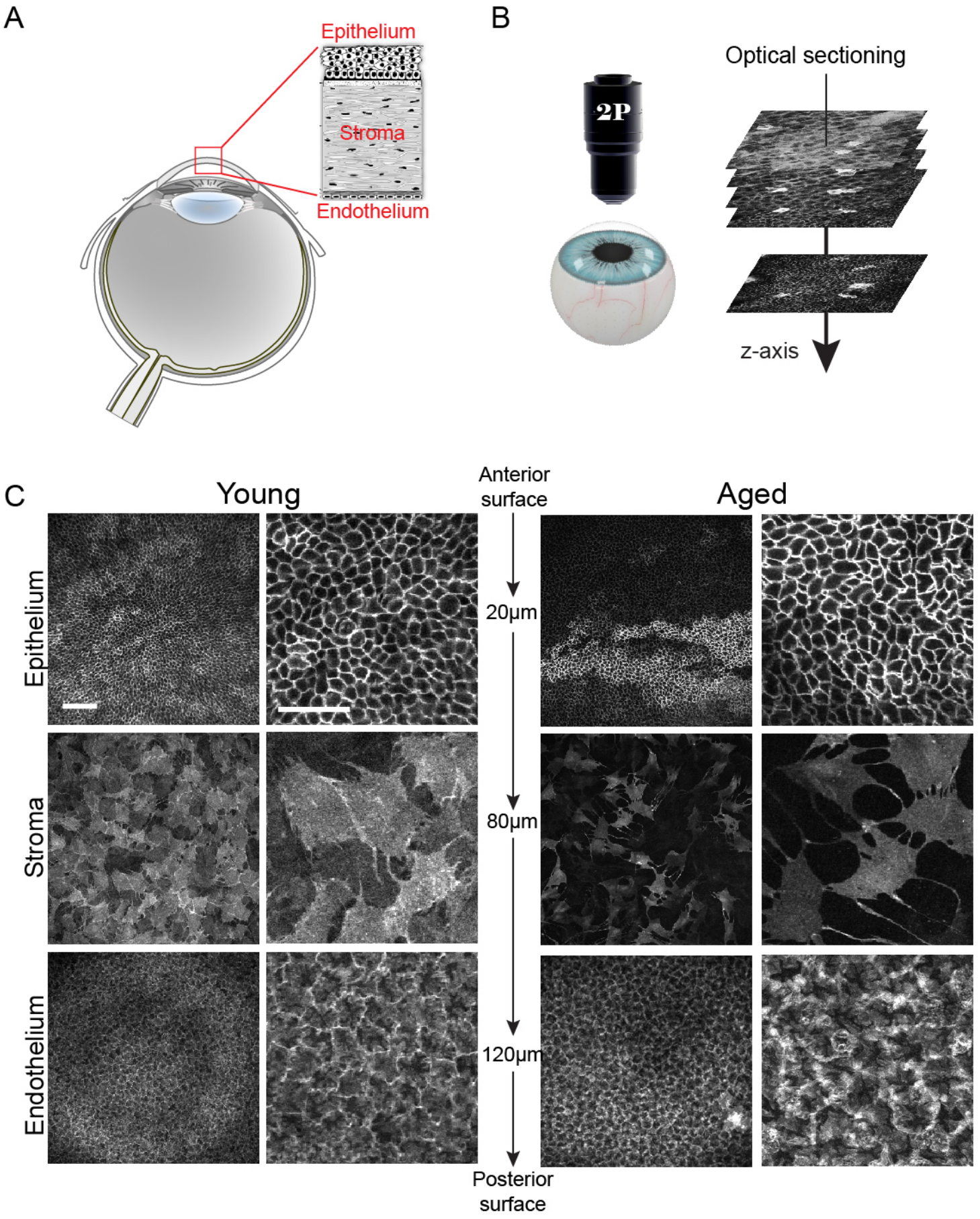

Supplementrary figure 2

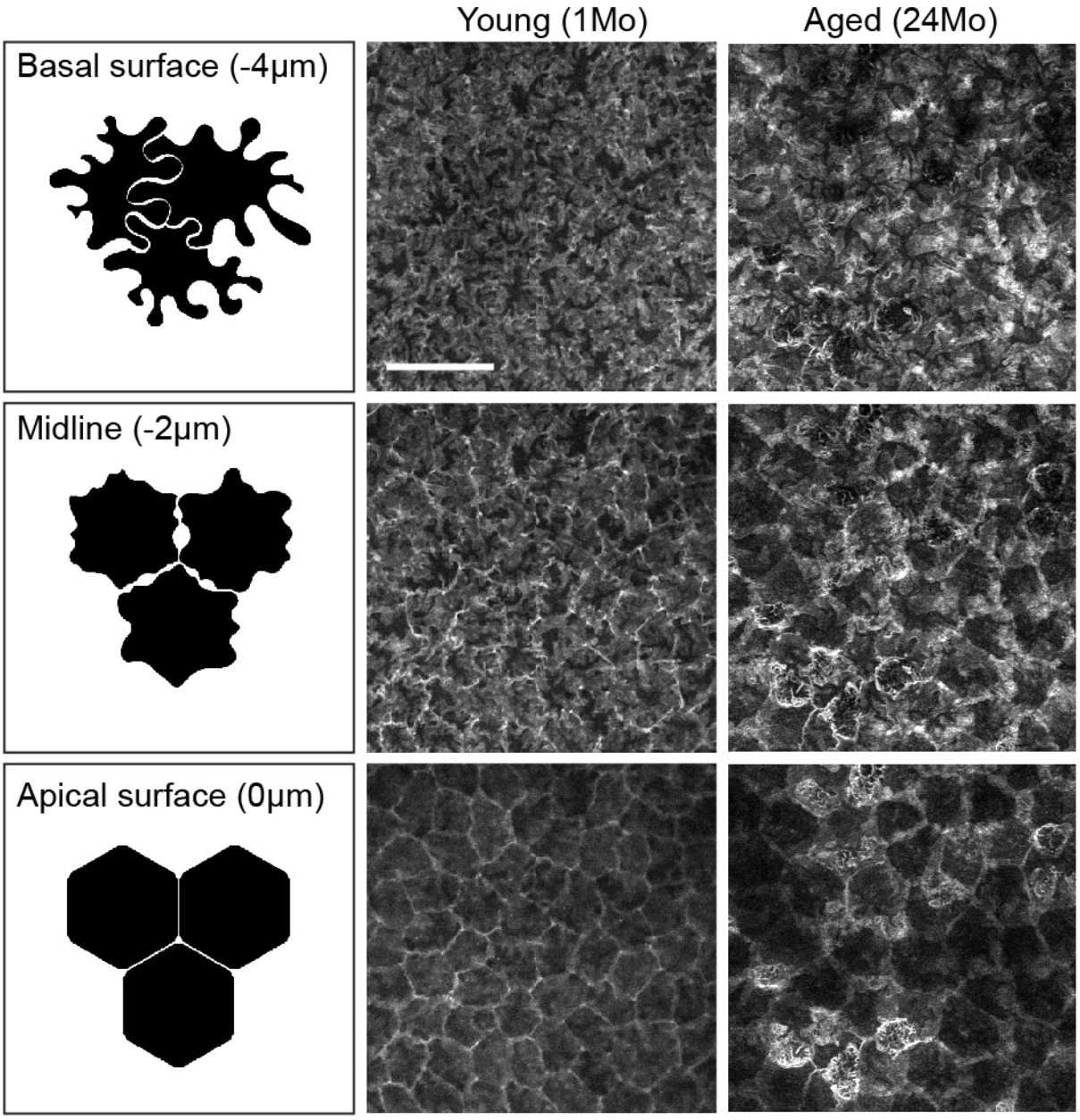

Supplementrary figure 3

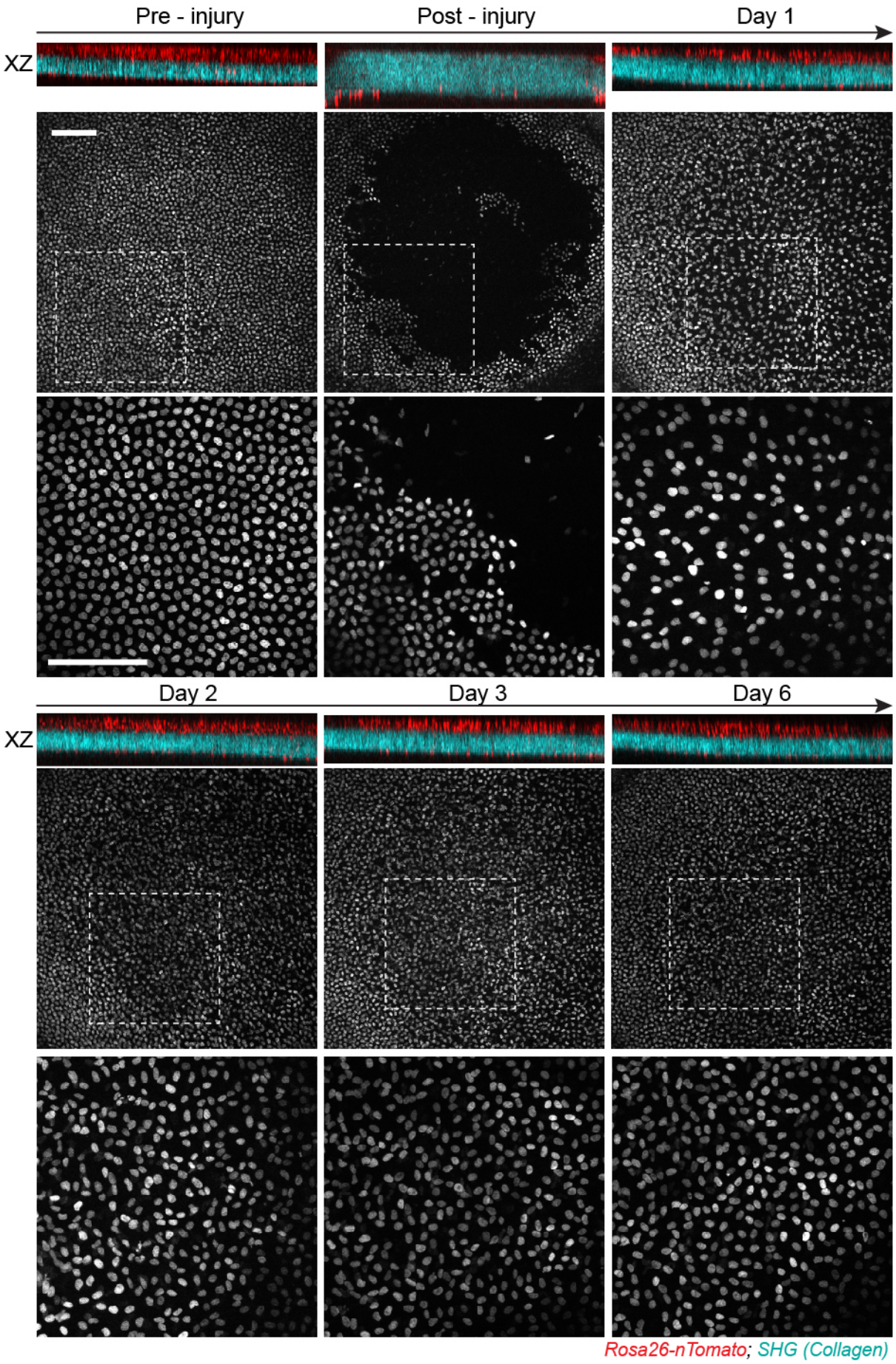

Supplementrary figure 4

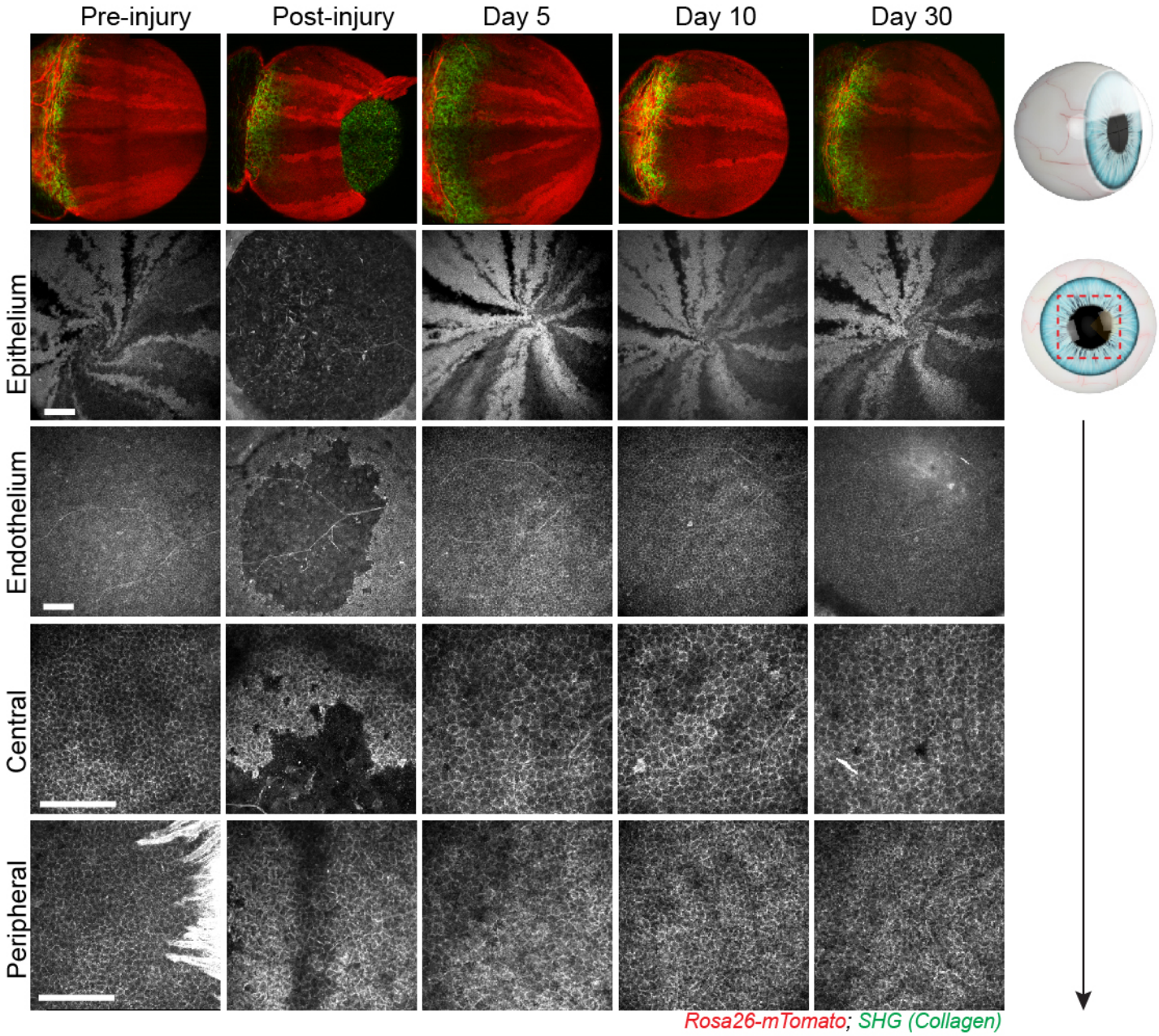

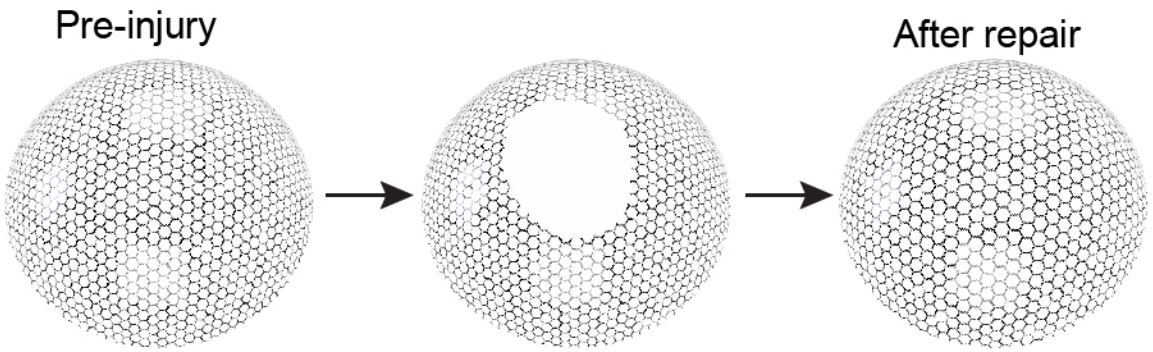

Supplementrary figure 5

A

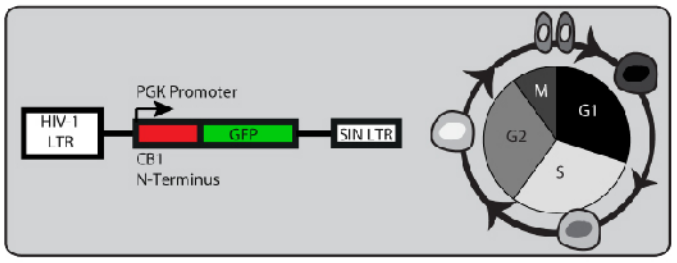

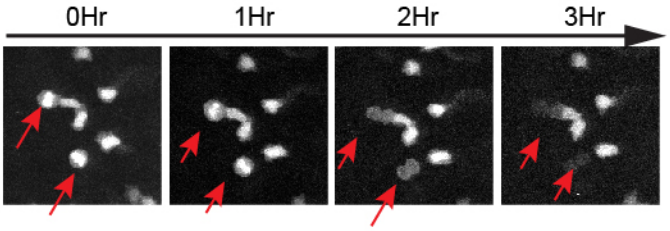

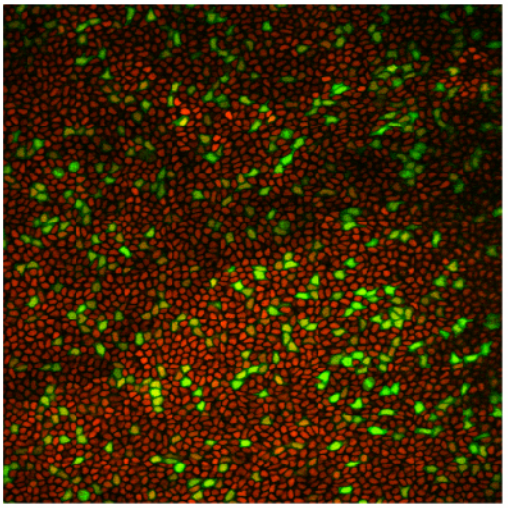

B

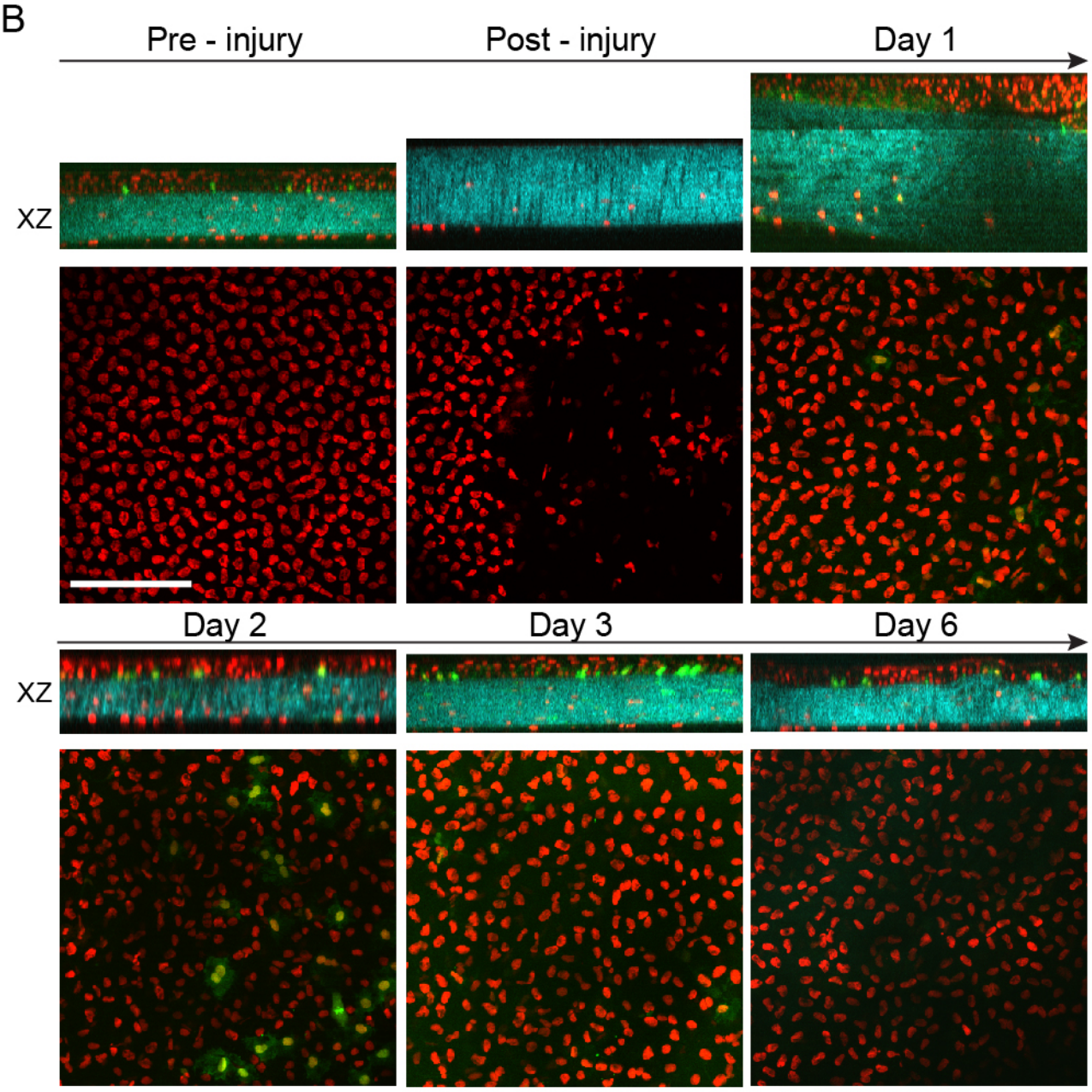

Rosa26-nTomato; *CycllinB1-GFP*; *SHG (Collagen)*

Supplementrary figure 6

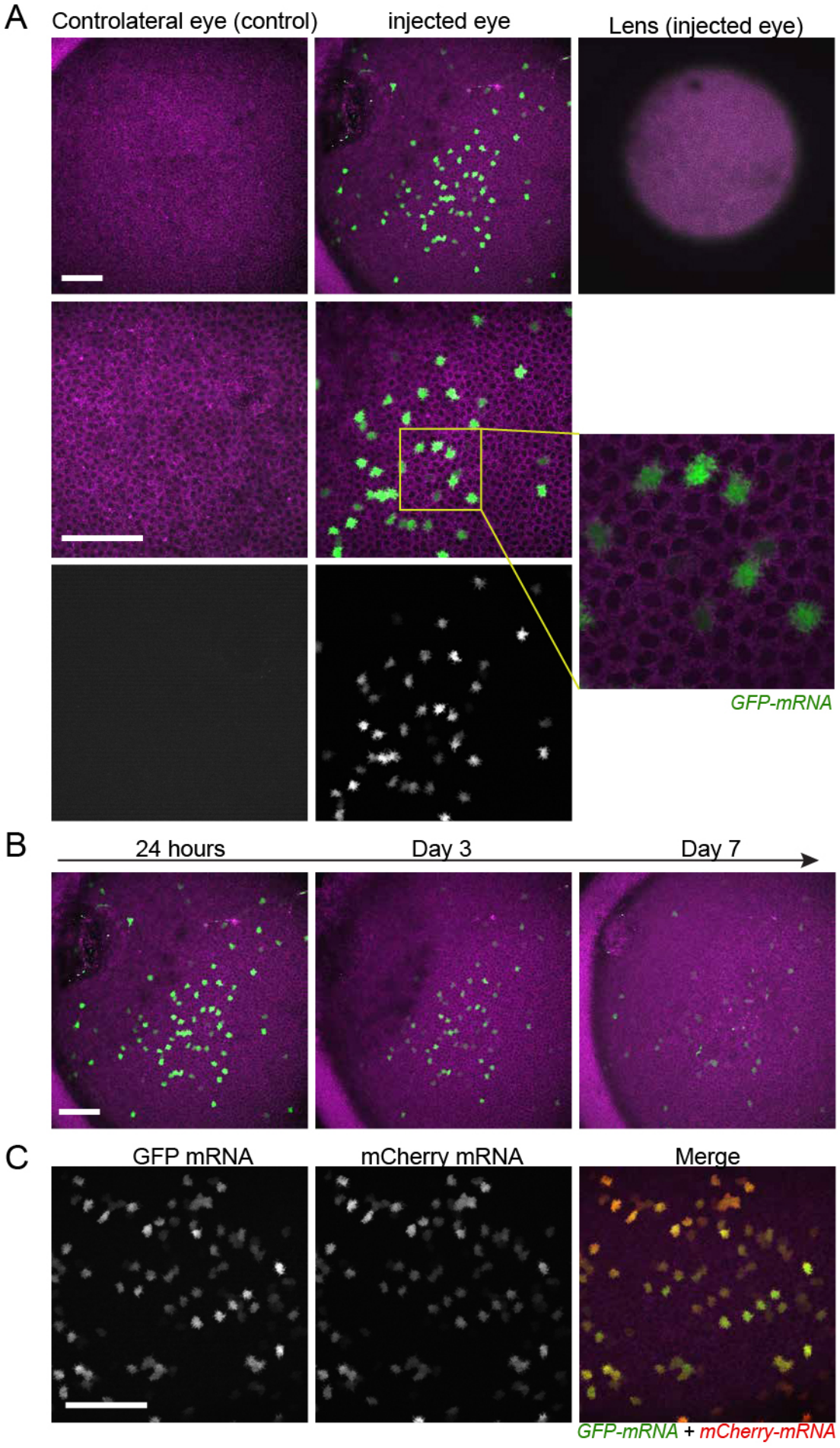

Supplementrary figure 7

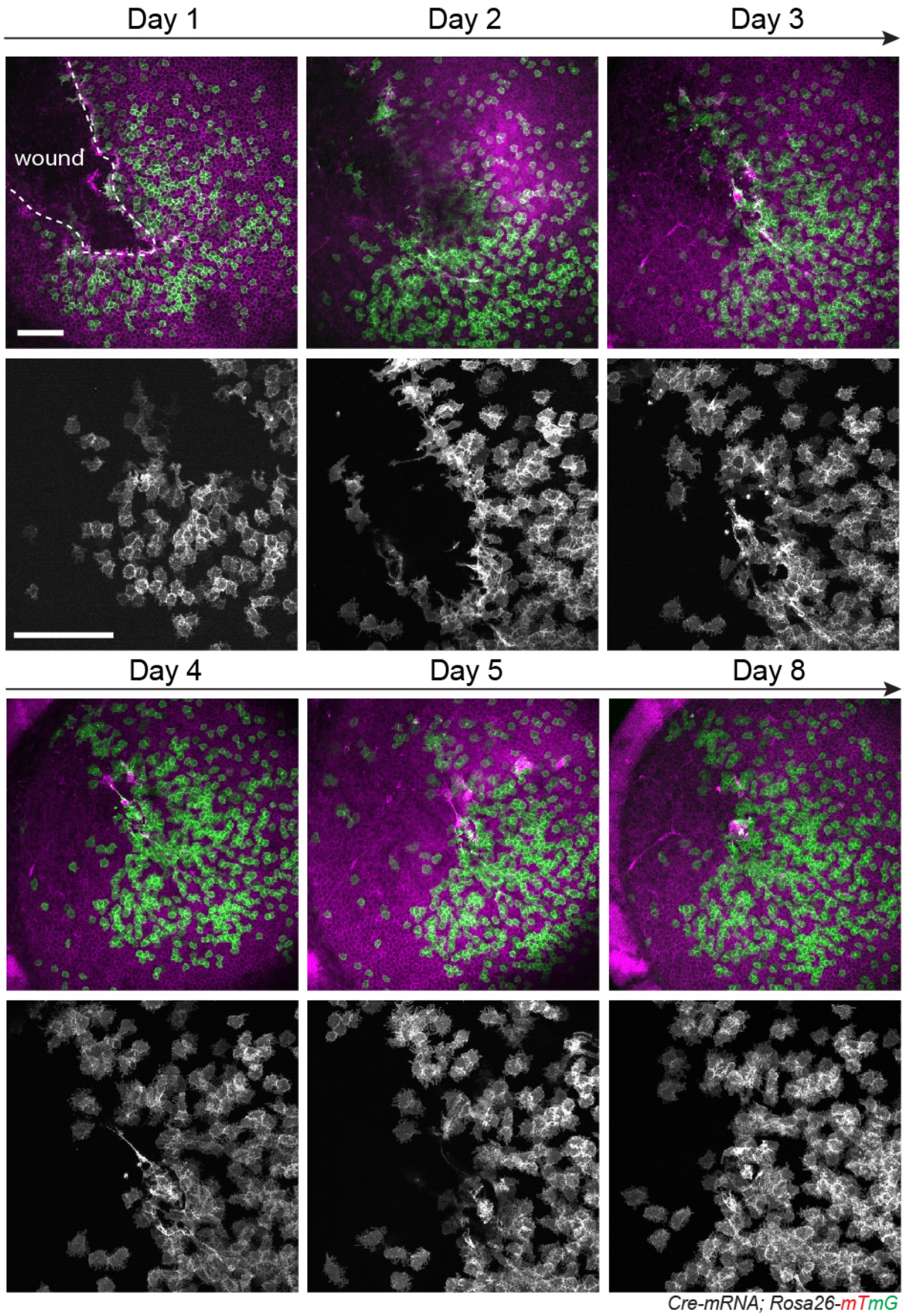

Supplementrary figure 8

A

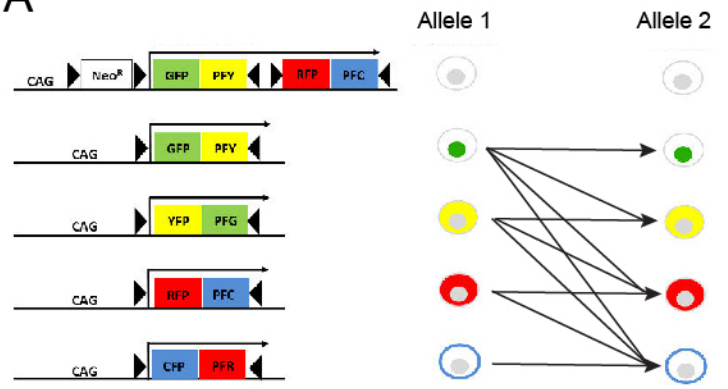

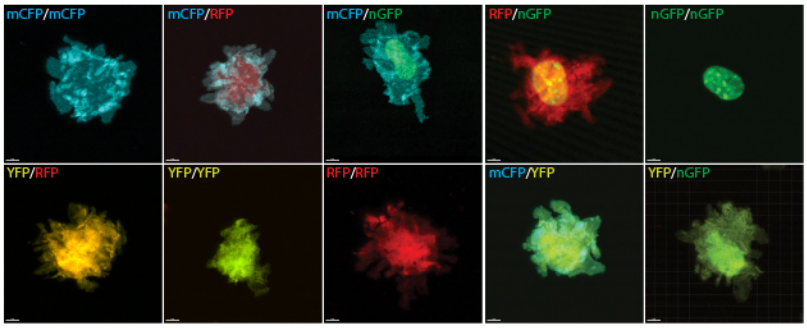

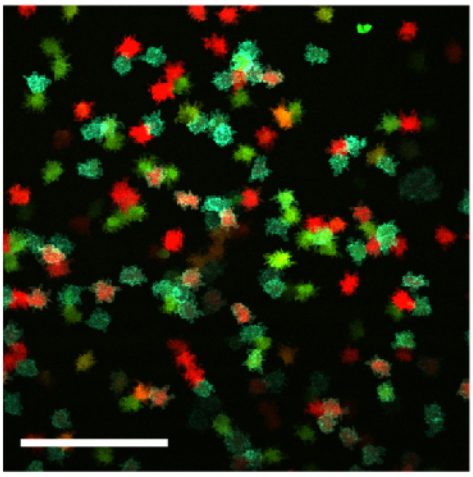

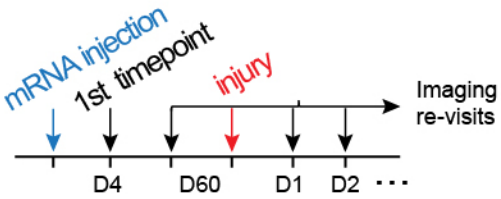

B

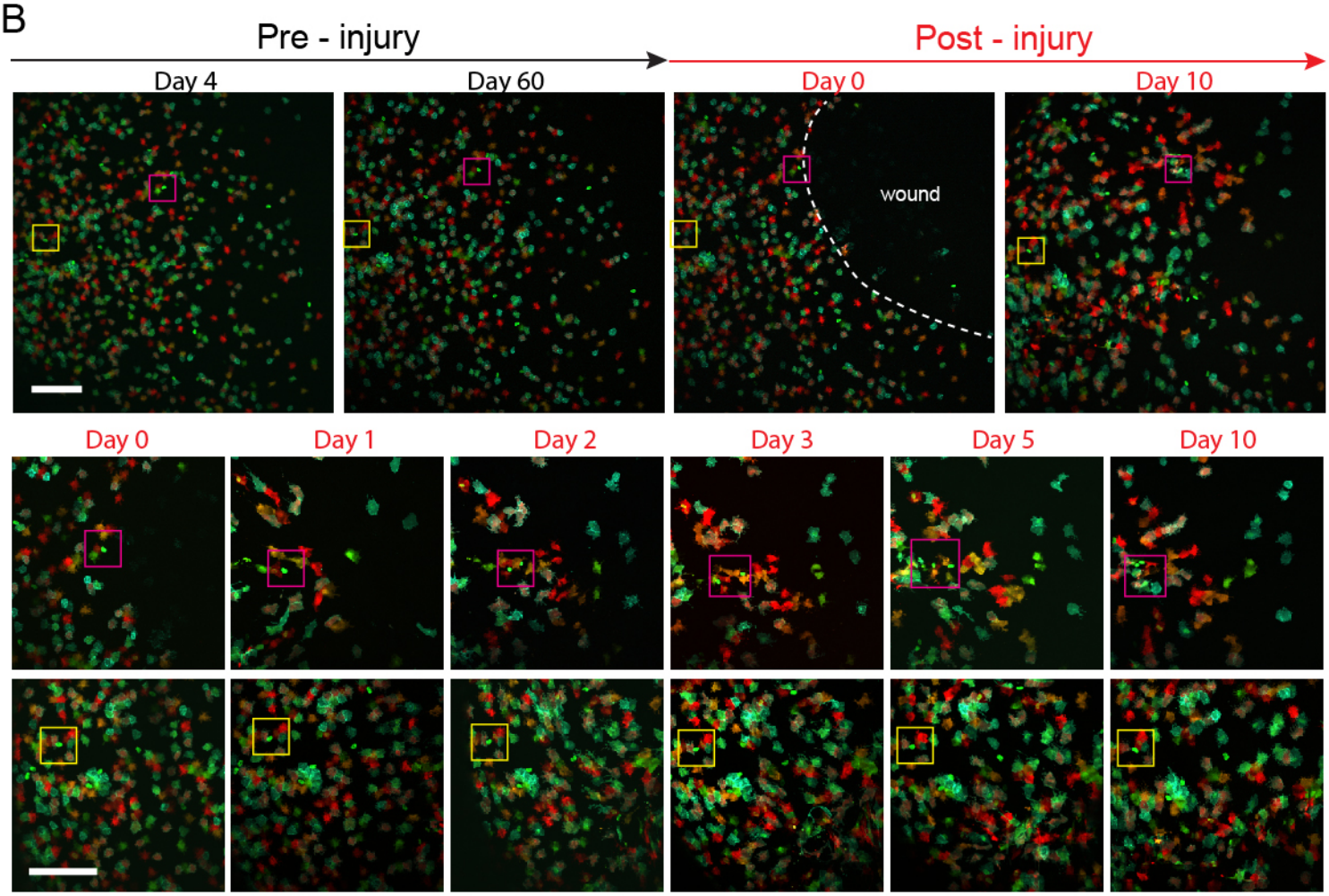

Supplementrary figure 9

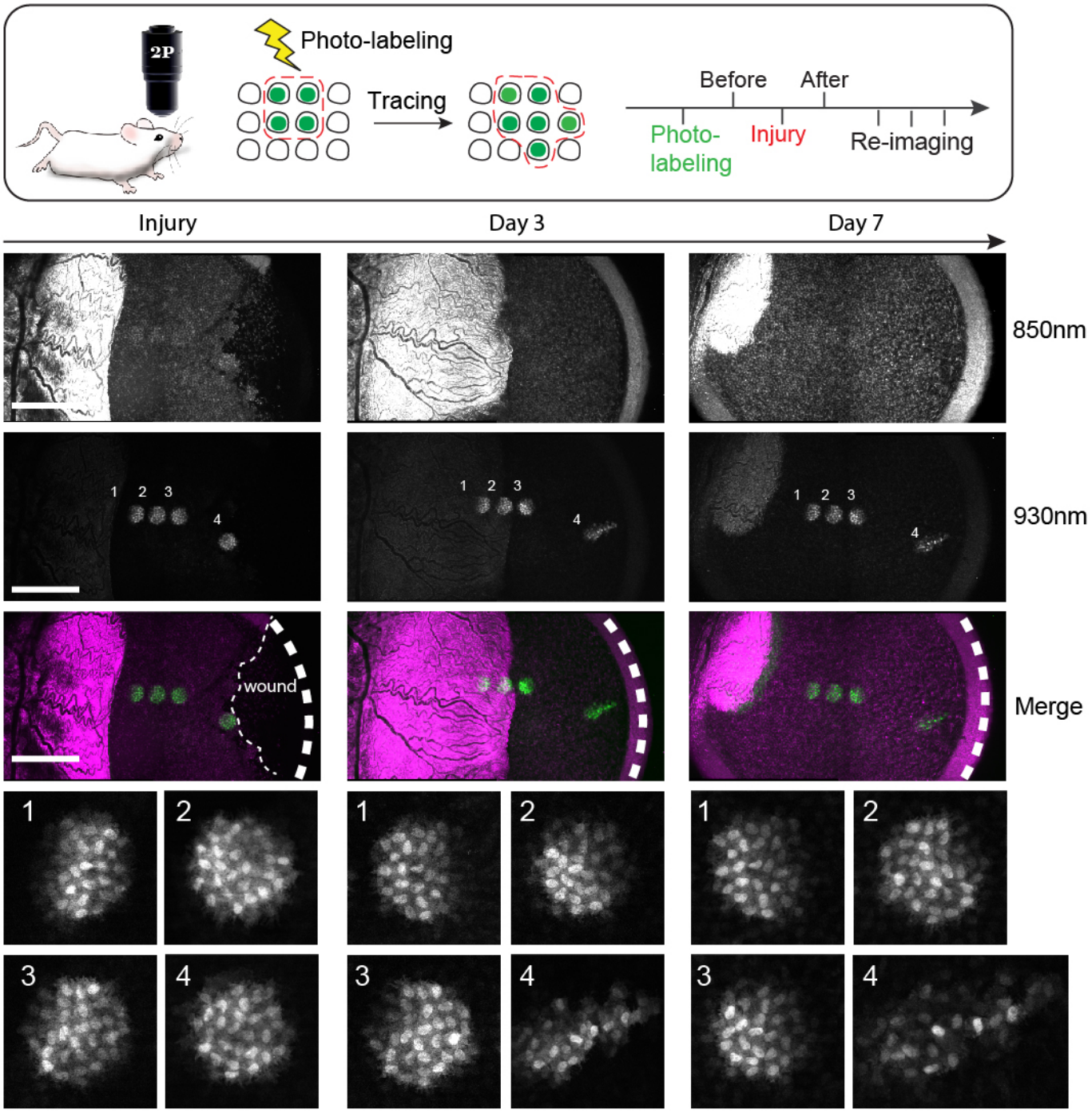

Supplementrary figure 10

A

5' aptamer sequence: G A C T C A C T A T T T G T T T T C G C G C C C A G T T G C A A A A A G T G T C G C C A C C A T G

3' UTR sequence: TGACAAGCACGCAGCAATGCAGCTCAAAACGCTTAGCCTAGCCACACCCCCACGGGAAACAGCAGTG
ATTAACCTTTAGCAATAAACGAAAGTTTAACTAAGCTATACTAACCCCAGGGTTGGTCAATTTCGTGCCAG
CCACACCCTGGTACTGCATGCACGCAATGCTAGCTGCCCCTTTCCCGTCCTGGGTACCCCGAGTCTCC
CCCGACCTCGGGTCCCAGGTATGCTCCCACCTCACCTGCCCCACTCACCACCTCTGCTAGTTCCAGAC
ACCTCCAAAAAAAAAAA....

B

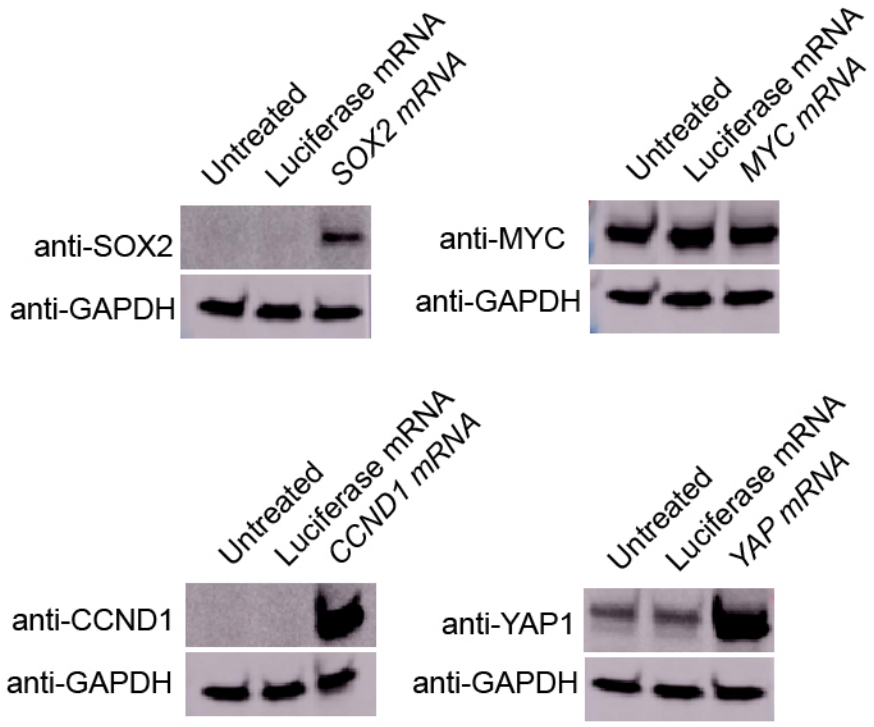

Supplementrary figure 11

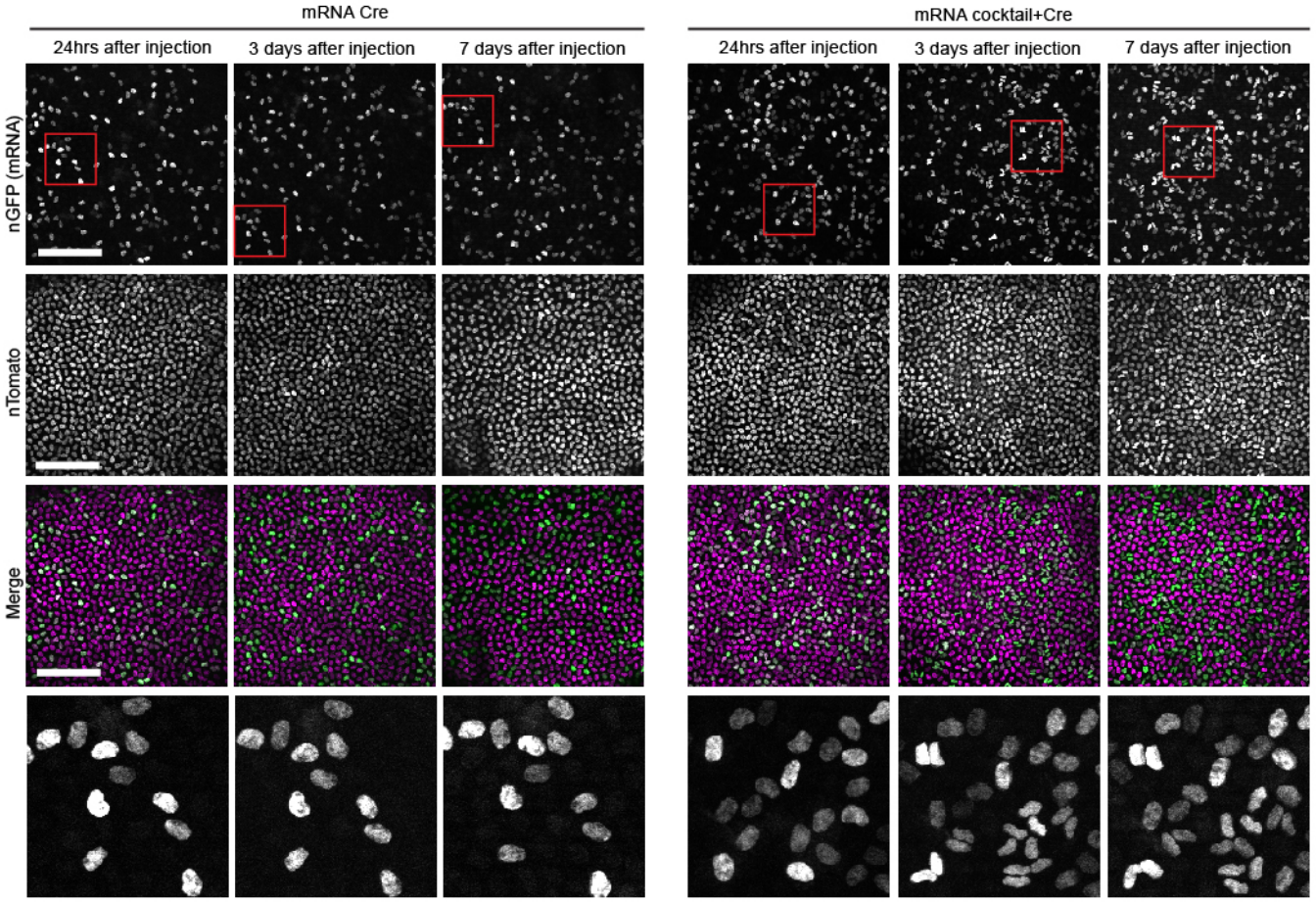
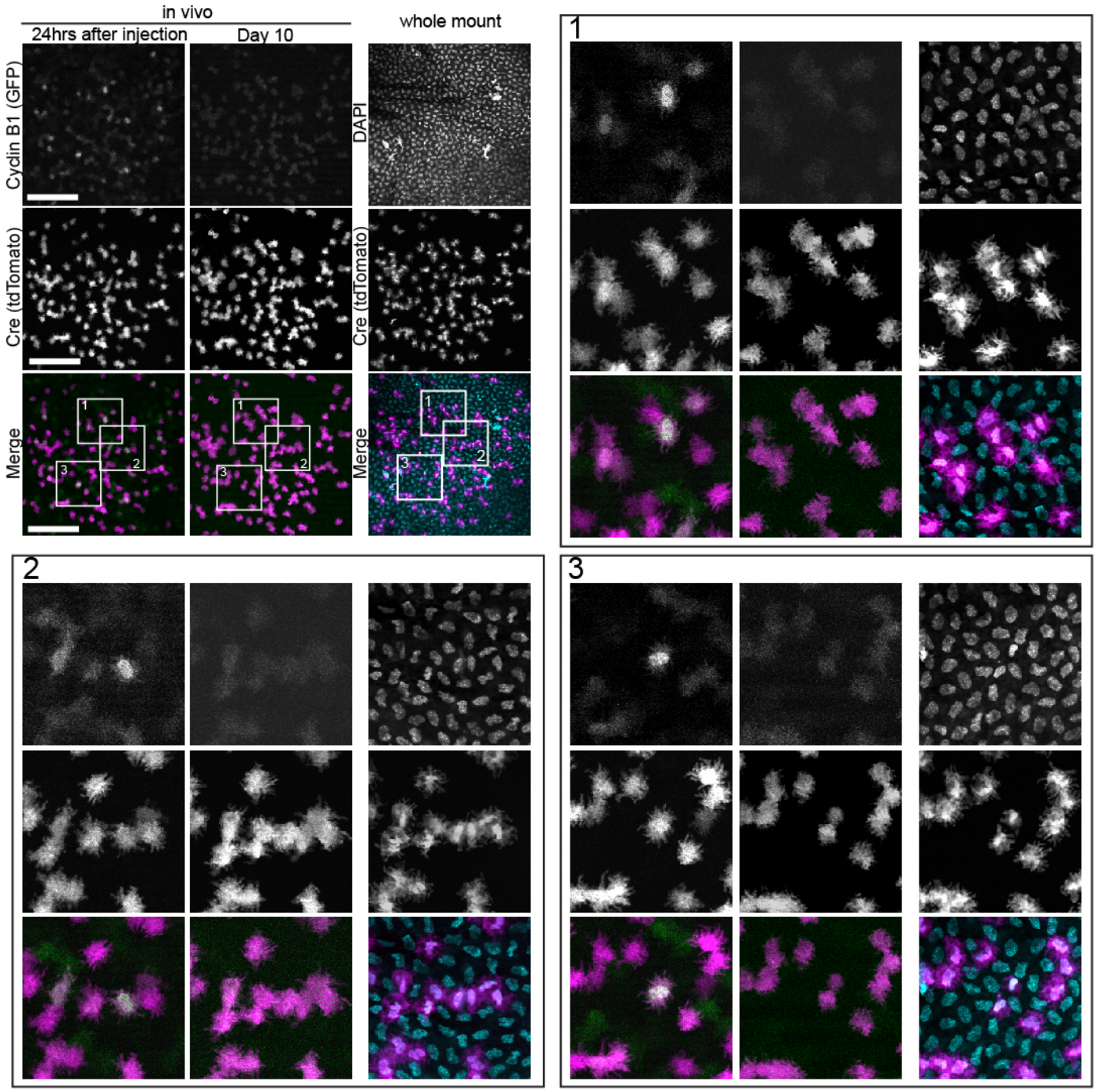
Supplementrary figure 12